Mechanisms of Pathogenicity of Hypertrophic Cardiomyopathy-Associated Troponin T (TNNT2) Variant R278C$^{+/-}$ During Development

Sanam Shafaattalab[1,2,α], Alison Y Li[1,2,α], Farah Jayousi[1,2,α], Yasaman Maaref[1,2,α], Saif Dababneh[1,3,α], Homa Hamledari[1,2], Dina Hosseini Baygi[1,2], Tiffany Barszczewski[1,2], Balwinder Ruprai[1,2], Shayan Jannati[1,4], Raghu Nagalingam[1,2], Austin M Cool[5], Paulina Langa[6], Mu Chiao[4], Thomas Roston[7], R John Solaro[6], Shubhayan Sanatani[1], Christopher Toepfer[8], Steffen Lindert[4], Philipp Lange[9,10], Glen F Tibbits[1,2,11,12*]

[α]These authors contributed equally to this study

1. Cellular and Regenerative Medicine Centre, BC Children's Hospital Research Institute, Vancouver, BC, V5Z 4H4, Canada
2. Biomedical Physiology and Kinesiology, Simon Fraser University, Burnaby, BC, V5A 1S6, Canada
3. Department of Cellular and Physiological Sciences, Faculty of Medicine, University of British Columbia, Vancouver, BC, V6T 1Z3, Canada.
4. Mechanical Engineering, University of British Columbia, Vancouver, BC, V6T 1Z4, Canada
5. Department of Chemistry and Biochemistry, Ohio State University, Columbus, OH, USA
6. Department of Physiology and Biophysics, College of Medicine, University of Illinois at Chicago, Chicago, IL, 60612, USA
7. Division of Cardiology and Centre for Cardiovascular Innovation, The University of British Columbia 1081 Burrard Street, Level 4 Cardiology Vancouver, BC, V6Z 1Y6, Canada
8. University of Oxford, Oxford, UK
9. Pathology and Laboratory Medicine, University of British Columbia, Vancouver, BC
10. Michael Cuccione Childhood Cancer Research Program, BC Children's Hospital Research Institute, Vancouver, BC, V5Z 4H4, Canada
11. Molecular Biology and Biochemistry, Simon Fraser University, Burnaby, BC, V5A 1S6, Canada
12. School of Biomedical Engineering, University of British Columbia, Vancouver, BC, V6T 1Z3, Canada

*Correspondence:
Glen F Tibbits, PhD
Cellular and Regenerative Medicine Centre
BC Children's Hospital Research Institute
938 West 28th Avenue
Vancouver, BC, V5Z 4H4
Canada

tibbits@sfu.ca

Abstract

Hypertrophic cardiomyopathy (HCM) is one of the most common heritable cardiovascular diseases and variants of *TNNT2* (cardiac troponin T) are linked to increased risk of sudden cardiac arrest despite causing limited hypertrophy. In this study, a *TNNT2* variant, R278C$^{+/-}$, was generated in both human cardiac recombinant/reconstituted thin filaments (hcRTF) and human- induced pluripotent stem cells (hiPSCs) to investigate the mechanisms by which the R278C$^{+/-}$ variant affects cardiomyocytes at the proteomic and functional levels. The results of proteomics analysis showed a significant upregulation of markers of cardiac hypertrophy and remodeling in R278C$^{+/-}$ vs. the isogenic control. Functional measurements showed that R278C$^{+/-}$ variant enhances the myofilament sensitivity to Ca^{2+}, increases the kinetics of contraction, and causes arrhythmia at frequencies >75 bpm. This study uniquely shows the profound impact of the *TNNT2* R278C$^{+/-}$ variant on the cardiomyocyte proteomic profile, cardiac electrical and contractile function in the early stages of cardiac development.

Translational Perspective

Hypertrophic cardiomyopathy (HCM) is the leading known cause of sudden cardiac arrest in the young. Thin-variant associated HCM variants make up to 15% of familial HCM yet their molecular mechanisms remain less clear relative to thick filament variants. Here, we employ computational modeling, human cardiac recombinant/reconstituted thin filaments (hcRTF), and hiPSC-CMs to study the thin filament *TNNT2* R278C$^{+/-}$ variant, revealing its extensive pathogenicity and potential mechanisms by which it can lead to HCM and sudden death. Mavacamten, the recently FDA-approved treatment, was effective in alleviating contractile dysfunction in *TNNT2* R278C$^{+/-}$ hiPSC-CMs, positing it as a potential therapy for thin filament HCM.

62 **Graphical Abstract**

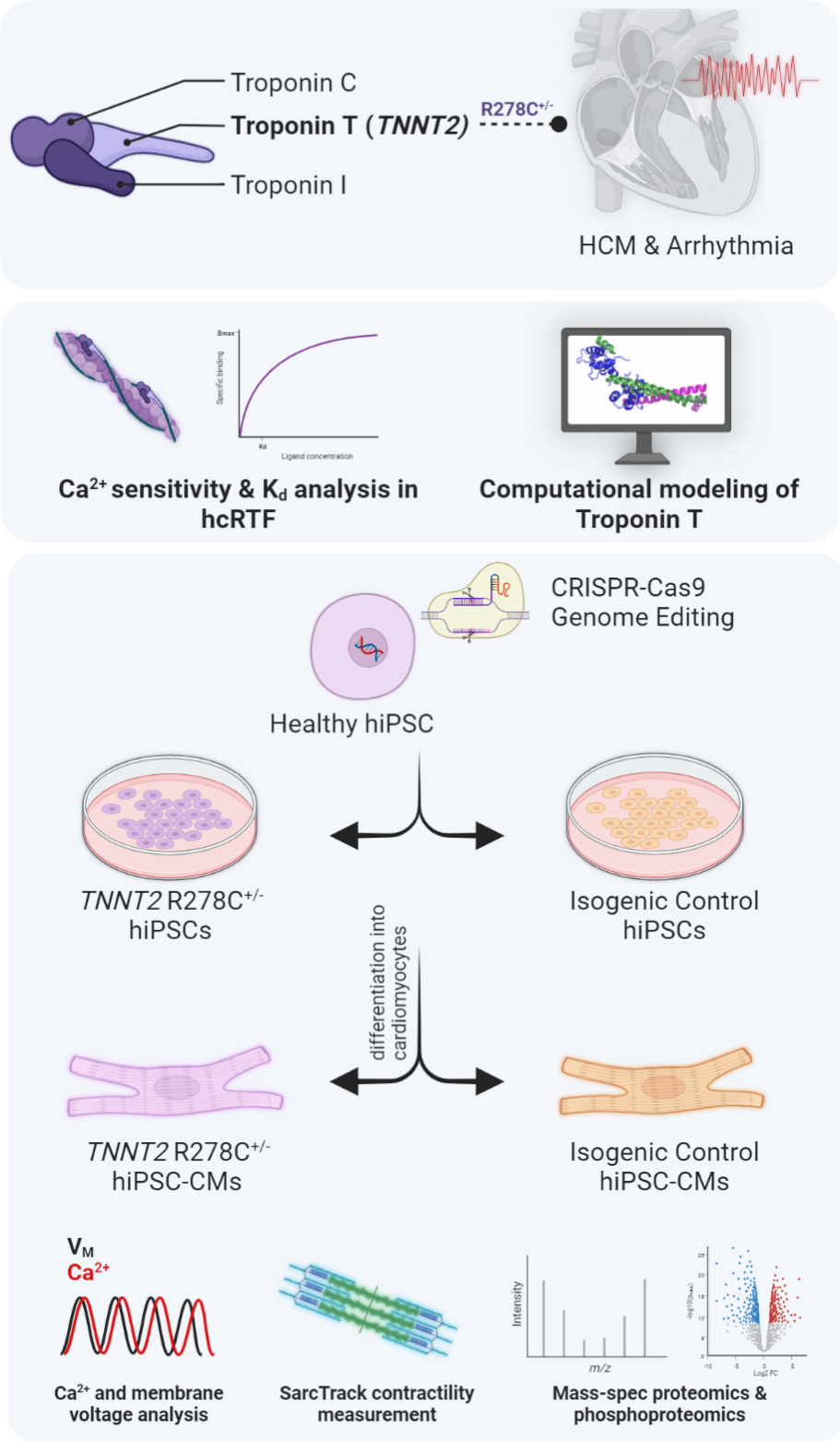

63

1. INTRODUCTION

Hypertrophic cardiomyopathy (HCM) is one of the most common inherited heart diseases and is associated with >1500 variants located in ~20 genes with the majority encoding for sarcomeric and Z-disc proteins[1]. HCM is an autosomal dominant inherited disorder that is characterized by asymmetrical left ventricular hypertrophy, enhanced contractility, impaired relaxation, and myofibrillar disarray, which clinically can manifest sudden cardiac arrest (SCA)[2,3]. The most common variants are in sarcomeric genes encoding the thick filament proteins cardiac myosin-binding protein C (*MYBPC3*) and β-myosin heavy chain (*MYH7*). However, variants in thin filament encoding proteins, such as *TNNT2*, make up 5-15% of HCM cases yet their pathogenic mechanisms remain relatively less clear[4,5]. Moreover, whether mavacamten, the allosteric myosin ATPase inhibitor recently approved by the FDA to treat obstructive HCM, would be effective in *TNNT2* variant carriers has yet to be studied.

Variants in *TNNT2* represent up to 50% of all thin filament HCM cases, with 400 unique TNNT2 variants have been identified in HCM patients[5,6]. In particular, the *TNNT2* R278C variant has been reported in over 50 unrelated patients with a clinical diagnosis of HCM [7,8], and is enriched in the HCM population compared to the general population[9]. Patients carrying this variant tend to present with relatively later-onset and milder hypertrophy compared to patients with *MYH7* and *MYBCP3* associated HCM but may have a higher risk of sudden cardiac death at young ages[10–15]. However, conflicting results from several mechanistic studies in patient myectomy tissue and animal models and the presence of multiple potentially disease-associated variants in some affected individuals have raised uncertainty as to the pathogenicity of the *TNNT2* R278C variant.

Genetic variants associated with HCM can result in dramatic defects in the biophysical dynamics of Ca^{2+} handling and contractility[3,16,17], which signal significant alterations in the transcriptome, proteome, and function. Recent studies have used hiPSC-CMs based disease models to investigate the underlying causes and consequences of HCM-linked variants[18,19]. We have previously shown that the HCM-associated *TNNT2* I79N$^{+/-}$ variant can enhance myofilament Ca^{2+} sensitivity by decreasing the Ca^{2+} off rate constant, alter the action potential morphology, and modify contractile kinetics in human iPSC-CMs[20].

Given the conflicting evidence of pathogenicity and the paucity of studies on the *TNNT2* R278C$^{+/-}$ variant in a human-based model, we sought to investigate R278C$^{+/-}$ using human iPSC-CMs and human cardiac recombinant/reconstituted thin filaments (hcRTF). There is compelling evidence that the arginine at residue 278 is highly conserved over four million years of evolution (Figure S1), with several variants at this residue considered pathogenic[10,21]. Moreover, our molecular mechanics potential energy minimization calculations strongly suggest the R278C$^{+/-}$ variant alters the interaction of *TNNT2* with tropomyosin (Tm) (Figure 1). Using hcRTF, we found that R278C$^{+/-}$ increased myofilament Ca^{2+} sensitivity. We then generated heterozygous *TNNT2* R278C$^{+/-}$ hiPSC-CMs and isogenic controls and conducted electrophysiological, contractile, and proteomic analyses. R278C$^{+/-}$ hiPSC-CMs showed various proteomic changes consistent with HCM such as myofibrillar disarray, hypercontractility, and a fetal-like metabolic switch. Using the MATLAB

103 based algorithm SarcTrack[22], we found sarcomere shortening, contraction, and relaxation kinetics
104 to be disrupted in R278C$^{+/-}$ hiPSC-CMs, which were alleviated in part by mavacamten. Lastly,
105 optical mapping showed a higher propensity for arrhythmias induced by the R278C$^{+/-}$ variant in
106 hiPSC-CMs. This unique approach in studying the early impact of the *TNNT2* HCM-related variant
107 R278C$^{+/-}$ on cardiomyocytes has generated a magnitude of novel data that could be impactful on
108 understanding this disease.

109

2. METHODS

2.1 Computational Modelling and Potential Energy Minimization

To obtain a model of the thin filament complex, the PDB structures 6KN7 (Ca^{2+} free) and 6KN8 (Ca^{2+} bound) were used[23]. Each of these structures contains two troponin complexes, with cardiac troponin T (cTnT) being designated as chains "a" and "T", respectively. Both cTnT chains have contacting actin and tropomyosin subunits, in which chain a is close to chains G (actin) and P (tropomyosin) and chain T is close to chains F (actin) and W (tropomyosin). None of the four TnT structures (6KN7a, 6KN7T, 6KN8a, and 6KN8T) contains residue R278, with each cTnT structure being truncated at residue Q272.

Rosetta was utilized to build residues 273-281, using the sequence: KVSKTRGKA. Each of the four TnT chains (6KN7a, 6KN7T, 6KN8a, and 6KN8T) was removed from the thin filament complex and 1,000 models were built of the existing structure plus residues 273-281 using the loop modeling application of Rosetta[24,25]. This was done twice, the first designated all the residues to be built as a helical structure, the second designated all the residues to be built as an unstructured loop. In both cases, Rosetta built residues 273-281 as a helical structure. The top scoring model was then placed into its original PDB structure to generate a thin filament model that contained the cTnT R278 residue.

Four more models were then created by introducing the $R278C^{+/-}$ variant into the models produced by Rosetta. Each of the eight models of the thin filament complex were then solvated with explicit TIP3W water molecules and NaCl counterions were added to neutralize the entire system and establish a final salt concentration of 150 mM. The resulting models were subjected to two sequential 10,000 potential energy minimization steps using Nanoscale Molecular Dynamics (NAMD) in the Charmm36 force field. This was done to optimize the positions of the solvent molecules around the protein and to subsequently relax the positions of residue side chain atoms. To analyze the models, residues that were within a certain cutoff of the gamma carbon (CG) atom of the R278 residue of the native structure and of the gamma sulfur (SG) atom of the C278 residue in the mutated models, were recorded.

2.2 Generation of human cardiac reconstituted thin filaments (hcRTF)

Recombinant human adult troponin subunits were used to generate the cardiac troponin complexes (cTn). Recombinant human α-Tm produced in E. coli does not undergo an acetylation process and the unacetylated initial Met binds actin poorly and does not polymerize. In this study, the recombinant αTm included an MAS peptide (Met-Ala-Ser) added to the N-terminus to mimic the acetylation process and ensure actin binding[26]. The purification of each protein was verified by gel electrophoresis. Reconstituted thin filaments were then generated by mixing each cTn complex with human αMAS TPM1 as well as native actin extracted from rabbit skeletal muscle which has a 99.2% sequence identity with human cardiac actin[27]. The stopped flow assay used for testing the functional validity of the hcRTF in this study has been described by Davis et *al.* [28].

148 **2.3 Determination of hcRTF Ca^{2+} kinetics**

149 The Ca^{2+} off rate constants (k_{off} (Ca^{2+})) from each hcRTF were characterized using a Chirascan
150 stopped-flow apparatus (Applied Photophysics, Surrey, UK) with a dead time of 1.1 ms at 15.0 ±
151 0.1°C. 2-(4'-(iodoacetoamido)anilino) naphthalene-6-sulfonic acid (IAANS) fluorophore was
152 attached to residue C53 of TnC, was excited at 300 nm and monitored through a 510 nm broad
153 band-pass interference filter (Semrock, Rochester, NY) as described by Davis *et al.*[28]. Each trace
154 was obtained as the solution containing hcRTF saturated with 200 µM CaCl2 was rapidly mixed
155 with 10 mM EGTA solution in the stopped-flow buffer containing (in mM): 10 MOPS, 150 KCl, 3
156 MgCl2, 1 DTT, pH 7.0. Each k_{off}(Ca) value represents an average of at least five traces fit with a
157 single exponential equation and repeated more than 15 times. Two means were considered to be
158 significantly different when $p < 0.05$.

159 All steady-state fluorescence measurements were performed using a Cary Eclipse fluorescence
160 spectrophotometer (Agilent, Santa Clara, CA) at 15 ± 0.1°C. In brief, the IAANS fluorophore was
161 excited at 330 nm and monitored at the peak of the emission at 450 nm. Microliter amounts of
162 $CaCl_2$ were added to 2 mL of each labeled hcRTF in a titration buffer containing (in mM): 200
163 MOPS, 150 KCl, 3 MgCl2, and 1 DTT at pH 7.0. At least five to eight datasets were collected for
164 each construct and the data were fit with a sigmoidal fit (based on the Hill equation) in Origin 8.5
165 (Microcal Software, Northampton, MA). The Ca^{2+} sensitivity for each hcRTF was represented by
166 the dissociation constant K_d (± SEM) defined as the Ca^{2+} concentration at the half-maximal
167 fluorescence change. Two means were significantly different when $p < 0.05$.

168 **2.4 Human iPSC maintenance and cardiomyocyte differentiation**

169 Human iPSC lines were obtained from the Wicell Research Institute (iPS IMR90-1)
170 (https://www.wicell.org/) and the Allen Institute (https://alleninstitute.org/). Differentiation of
171 hiPSCs to ventricular cardiomyocytes (hiPSC-CMs) employed a protocol published previously. In
172 brief, hiPSCs were maintained on a Corning Matrigel (0.5 mg/ 6-well plate, dissolved in DMEM/F-
173 12 medium) cultured in mTeSR1 medium (StemCell Technologies, Vancouver, BC). Cells were
174 passaged every 4 days using Versene solution (ThermoFisher, Waltham, MA) and were then
175 seeded on a 6-well Matrigel-coated plate at a density of 100,000 cells cm-2 in mTeSR1 medium.
176 The medium was changed daily, and after 3 to 4 days, when the monolayer of cells reached >90%
177 confluency, the mTeSR1 medium was replaced with Roswell Park Memorial Institute Medium
178 (RPMI) 1640 basal medium (ThermoFisher, Waltham, MA) plus 2% B27 without insulin
179 supplement (ThermoFisher) containing 12 µM CHIR99021 (R&D Systems) for 24 h, followed by 5
180 mM IWP4 (Tocris) for 2 days without medium change. The medium was changed to RPMI 1640
181 plus B27 complete supplement, and then subsequently the medium was changed every 2 to 3
182 days. Robust spontaneous beating of the monolayers was observed by day 12.

183 **2.5 Preparation and design of CRISPR-Cas9 and donor template**

184 The single-guide RNAs (sgRNA) were prepared using online CRISPR tools including CRISPRko Tool
185 from the Broad Institute, the CRISPR Finder from Wellcome Trust Sanger Institute, and Benchling.
186 The sgRNA sequences were designed to target the region close to R278 residue of *TNNT2* as

shown in Figure S2. They were then cloned into a pCCC vector which is based on pSpCas9(BB)-2A-GFP vector (PX458, Addgene plasmid # 48138). The pCCC vector contains the complete U6 promoter for enhanced expression in hiPSCs. The 127 bp asymmetric single- stranded donor nucleotides (ssODNs)[29,30] were designed (Figure S2) to include the transitions (T -> A) and (C -> T) that are seen in R278C as well as a silent mutation at the PAM site to prevent the continuous cutting and improve the efficiency of the HDR repair.

2.6 Transfection and Fluorescence-Activated Cell Sorting (FACS)

Human iPSCs were co-transfected with the R278C-sgRNA-pCCCplasmid and the ssODN donor template using Lipofectamine 3000 (ThermoFisher). Briefly, 2 × 105 hiPSCs were transfected with 500 ng sgRNA plasmid and 10 pmol of ssODN. Since the vector contained GFP as a reporter, the GFP+ hiPSCs were sorted as single cells using Fluorescence-Activated Cell Sorting (FACS) 48–72 hours post-transfection and were plated on Matrigel-coated plates in mTeSR122. More than 100 single-cell colonies were genotyped. To screen for on-target single mutation, genomic DNA was extracted (DNEasy, Qiagen, Mississauga, ON) and used for PCR amplification of the region around the CRISPR target sites. These amplicons were Sanger sequenced to confirm the single nucleotide mutation at the R278 *TNNT2* site using the primers described in Figure S2.

2.7 Protein isolation and quantification

The myocardial proteins were isolated from hiPSC-CM pellets (400k-500k cells) for both cell lines approximately 30 days after differentiation. The timely collection of the CMs was done using STEMdiff reagent from the CM dissociation kit (STEMCELL Technologies, Vancouver, BC). STEMdiff was added to each well of hiPSC-CMs, and after incubation with its neutralizing agent, the cells detached from the Geltrex matrix and were pipetted up and down for a homogenous suspension. This was followed by centrifugation of the collected cells to obtain a pellet of hiPSC- CMs. The pellet was then resuspended in lysis buffer according to the number of cells. The cells were counted using the CellDrop automated cell counter (Froggabio, ON). The lysis buffer used contained 100 mM HEPES (pH= 8-8.5) + 20% SDS, and 75 µL of were added per~ 2 million cells. Cell lysates were then placed for 5 minutes in 95°C water bath, followed by 3 minutes on ice. To complete the lysis, the samples were sonicated twice for 30 seconds, and placed on ice between rounds. This was followed by treatment with benzonase (EMD Millipore-Sigma) at 37°C for 30 min to fragment the chromatin.

After obtaining the CM lysate, each sample was reduced with 10 mM dithiothreitol (DTT) at 37 °C for 30 min, followed by alkylation with 50 mM chloroacetamide (CAA) for 30 min in the dark. The alkylation was quenched in 50 mM DTT for 10 min at room temperature. To clean the lysates, high-resolution sample-preparation (SP3) technology was the purification approach used to isolate the proteins in the samples. This protocol is a paramagnetic bead–based approach for rapid and efficient processing of protein samples before proteomic analysis[31]. SP3 uses a hydrophilic interaction mechanism for the removal of interfering components (e.g., detergents, salts, buffers, acids, and solvents). The magnetic beads facilitate a wide range of nonselective protein binding that is enabled through the use of an ethanol-driven solvation layer on the surface

226 of the beads. To each sample, hydrophilic and hydrophobic Sera-Mag Speed Beads (GE Life
227 Sciences, Washington, US) were added in 1:1 ratio. Proteins were then bound to the beads with
228 100% ethanol (80% v/v) and washed twice with 90% ethanol.

229 After binding of the proteins to the beads, the samples underwent an overnight enzymatic
230 digestion with trypsin (1:50 w/w), followed by C18 matrix midi-column clean up and elution. The
231 BioPure midi columns (Nest Group Inc.) were conditioned with 200 µL methanol, 200 µL 0.1%
232 Formic Acid (FA), 60% Acetonitrile (ACN), and 200 µL 0.1% Trifluoroacetic Acid (TFA). The pH of
233 the samples was adjusted to 3 – 4 using 10% TFA prior to loading the columns. Samples were
234 sequentially eluted 3 times with 70 µL, 70 µL, and 50 µL 0.1% FA, 60% ACN. The eluate was
235 collected into LoBind tubes and placed into a SpeedVac to remove the organic ACN. Lastly, the
236 samples were re-suspended in 0.1% FA (ready for MS injection). The total protein concentration
237 for each of the purified samples was determined using Nanodrop. Mass spectrometric analyses
238 were performed on Q Exactive HF Orbitrap mass spectrometer coupled with an Easy-nLC liquid
239 chromatography system (Thermo Scientific). This intricate system detects the ionized peptides at
240 the specific time that they elute out of the LC column (retention time). This time is calculated as
241 the period between injection to detection.

242 In the MS sample chamber (96-well plate), the samples were completely randomized across all
243 conditions and biological replicates. A total of 1 µg peptide per sample was injected for analysis.
244 The peptides were separated over a three-hour gradient consisting of Buffer A (0.1% FA in 2%
245 acetonitrile) and 2%-80% Buffer B (0.1% FA in 95% acetonitrile) at a set flow rate of 300 nL/min.
246 The computerized MS setup produces a pattern spectrum of masses based on the abundance and
247 structure of the detected ionized molecules.

248 The raw mass-to-charge (M/Z) data acquired from the Q Exactive HF were searched with
249 MaxQuant (MQ)-version 2.0.0.0 (Max Planck Institute, Germany), and Proteome discoverer
250 software (Thermo Fisher Scientific, CA, USA), using the built-in search engine, and embedded
251 standard DDA settings. The false discovery rate for protein and peptide searches was set at 1%.
252 Digestion setting were set to trypsin. Oxidation (M) and Acetyl (N-term) were set as dynamic
253 modifications. Carbamidomethyl (C) was set as fixed modification, and Phosphorylation (STY) was
254 set as a variable modification. For the main comparative protein search, the human proteome
255 database (FASTA) was downloaded from Uniprot (2022_06; 20,365 sequences) and used as the
256 reference file. Common contaminants were embedded from MaxQuant. Peptide sequences that
257 were labeled as "Potential contaminant/REV" were excluded from the final analysis.

258 **2.8 Optical mapping for action potential and calcium transient recordings**

259 Prior to imaging, monolayers of hiPSC-CMs ± R278C$^{+/-}$ were perfused with IMDM supplemented
260 with a physiological solution (final concentrations in mM): 140 NaCl, 3.6 KCl, 1.2 $CaCl_2$, 1 $MgCl_2$,
261 10 HEPES and 5.5 D-glucose for optical mapping as described[20,27,32,33]. In brief, the cells were
262 incubated with 15 µM of the potentiometric dye RH-237 (Molecular Probes, Eugene, OR) for 45
263 minutes. After incubating the hiPSC-CMs with RH-237, 5 µM of the Ca^{2+}-sensitive dye Rhod-2AM
264 (Molecular Probes), 20 µM blebbistatin (a myosin ATPase inhibitor (Sigma-Aldrich)) were added

265 to the culture dish. Blebbistatin inhibits contraction and reduces motion artifact with no
266 detectable effect on the electrophysiology properties[34,35]. For imaging, the hiPSC-CMs were
267 excited by 532 nm LEDs. RH-237 and Rhod-2 emissions were monitored using a >710 nm long-
268 pass and 565-600 nm band-pass filters, respectively, at 100 fps at 37°C. The spectral properties
269 allow both dyes to be fluoresced using 532 nm and their respective emissions to be separated by
270 dichroic mirrors. Both signals were captured with a single Hamamatsu ORCA Flash 4 digital CMOS
271 camera by incorporating an optical image splitter. Electrical field stimulation was applied using
272 stainless steel electrodes placed ~1 cm apart in the imaging chamber. The hiPSC-CMs harboring
273 the *TNNT2* heterozygous mutation R278C$^{+/-}$, and WT were stimulated for 20 seconds each at four
274 stimulation frequencies (55, 65, 75, and 100 beats/min). Data were analyzed using custom-built
275 software in IDL (Exelis Visual Information Solutions, McLean, VA)[27,32,33].

276 **2.9 Contractile parameters assessment using SarcTrack**

277 The contractile properties of both hiPSC-CMs ± R278C$^{+/-}$ were studied using SarcTrack[22] about 30
278 days after differentiation. SarcTrack facilitates high throughput contractile measurements of 2D
279 monolayers of hiPSC-CMs for disease modeling and large-scale pharmaceutical drug screening.
280 This MATLAB algorithm fits each sarcomere to a double wavelet with 6 definable parameters
281 including the distance between wavelet peaks as a function of time, constraint length of each
282 wavelet, width of each individual wavelet, number of angles that the wavelet test used to find
283 the best fit to the z-disc, distance between grid points to avoid refitting same sarcomere, and the
284 neighborhood around each grid where the best fit for the wavelet pair can be determined.
285 SarcTrack was used to measure the real time contractility of thousands of sarcomeres by running
286 multiple videos in parallel. The images were acquired with a Hamamatsu Orca Flash scMOS
287 camera at 100 frames per second (fps) to measure contractility in hiPSC-CM monolayers cultured
288 on PDMS matrices of 5 kPa tensile strength and stimulated at 1 Hz at 37℃. To image fluorescently
289 labeled sarcomeres, the α-actinin 2-GFP tagged hiPSC-CMs (Allen cell line (AICS-0075)) were used.
290 The images acquired at 100 fps resulted in good signal-to-noise ratio based on a root mean square
291 (RMS) analysis.

292 On day 14 of differentiation, WT and R278C$^{+/-}$ variant hiPSC-CMs were replated on a
293 Polydimethylsiloxane (PDMS) substrate with a stiffness of 5 kPa to provide a physiological
294 environment for the cells and to increase their maturation. To create a PDMS substrate with 5 kPa
295 elastic modulus, commercially available PDMS, Sylgard 527 gel (equal weights of part A and part
296 B) was used. The surface of PDMS substrate was coated with fibronectin (50 µg/ml) and hiPSC-
297 CMs were seeded with the concentration of 200,000 cell cm^{-2}. Two weeks after replating, the
298 samples were stimulated at 1 Hz frequency and 5 second videos were captured at 100 fps with
299 an ROI of 1024*1024 pixels. A Nikon Ti2 microscope was used with 100x oil immersion objective
300 and several videos were captured from different parts of the substrate. Next, by defining the
301 appropriate SarcTrack parameters, multiple videos were run simultaneously. To run more than
302 100 videos at the same time, the files were uploaded to the computational cluster at the Digital
303 Research Alliance of Canada. This advanced research computing system allows one to specify
304 different numbers of CPUs and decreases the computational cost. In this study, 32 CPUs were

305 defined to run more than 100 videos in about 10 hours. The measured contractility parameters
306 included the percentage of sarcomere shortening, time to half contraction, time to half relaxation,
307 maximum velocity of contraction, and maximum velocity of relaxation of WT and R278C$^{+/-}$ variant
308 hiPSC-CMs. To study the effect of mavacamten on the contractility parameters, R278C$^{+/-}$ variant
309 hiPSC-CMs were treated with 0.3, 1, and 3 µM mavacamten for 15 min before capturing videos.

310 **2.10 Statistical analysis**

311 Average data are provided as mean ± standard error of mean (SEM). The generated MS raw data
312 were filtered and transformed to log2 scale. This was followed by quantile normalization for all
313 samples. The proteomic profile for the HCM variant was subject to comparative analysis against
314 the isogenic control cell line. The protein groups file obtained from the DDA MQ search was used
315 for all the quantitative statistical analysis based on the detected intensities. All plots,
316 visualizations and statistical comparisons were done using R and Perseus (version 1.6.15.0)
317 software based on unpaired two tailed Student's t-test of significance. The level of significance
318 (p-value < 0.05) and number of data points (n) are indicated in each figure.

319

3. RESULTS

3.1 Computational potential energy minimization of WT and R278C$^{+/-}$ cardiac thin filament

Potential energy minimizations of our Rosetta models were carried out for the cardiac thin filament with and without and the R278C cTnT variant (Figure 1). The R278C$^{+/-}$ potential energy minimization analysis suggests that the substitution of a positively charged arginine to a more hydrophobic cysteine may cause more favorable local interactions. The residues in the actin and tropomyosin molecule that are within proximity of residue 278 of cTnT create a slightly positively charged environment. Therefore, the native R278, which is positively charged, may be less favorable to exist in this environment due to the charge repulsion compared to a mutated R278C. If this repulsion of an R278 residue is necessary for normal function (i.e., to provide some flexibility in the local region), we propose that the R278C mutation may disrupt this function due to the lack of the repulsion. In addition, there was no nearby cysteine from actin or Tm that could form any potential disulfide bridges with R278C.

With the cutoff set at 10 Å, five residues of Tm were within the range of the CG or the SG atom for all eight models: Arg167, Val170, Ile171, Ser174 and Arg178 (chain P/W). At this cutoff, the four 6KN7 CG/SG atoms of the models are within range of residues within the closest actin (F/G), whereas the four 6KN8 CG/SG atoms are not within range of any actin molecules. Analysis of this shows that the mutated R278C$^{+/-}$ models of 6KN7 are closer, by about 2 Å, to Arg147 and Thr148 of the actin molecule. Two representations of residue 278 (one in the wildtype actin chain F the second in the variant form) in its environment (with proximal actin/tropomyosin residues labeled) are shown in Figure 1)[36,37].

With the cutoff set at 10 Å, five residues of tropomyosin were within the range of the CG or the SG atom for all eight models: Arg167, Val170, Ile171, Ser174 and Arg178 (chain P/W). At this cutoff, the four 6KN7 CG/SG atoms of the models are within range of residues within the closest actin (F/G), whereas the four 6KN8 CG/SG atoms are not within range of any actin molecules. Analysis of this shows that the mutated R278C$^{+/-}$ models of 6KN7 are closer, by about 2 Å, to Arg147 and Thr148 of the actin molecule. Two representations of residue 278 (one in the wildtype actin chain F the second in the variant form) in its environment (with proximal actin/tropomyosin residues labeled) are shown in Figure 1[36,37].

3.2 Ca^{2+} sensitivity and dissociation rates in human cardiac reconstituted thin filaments (hcRTF)

Alterations to myofilament Ca^{2+} sensitivity are a hallmark of HCM-associated variants and can explain pathological changes seen in HCM such as hypercontractility and metabolic dysfunction[38]. To study this, steady-state fluorescence measurements were carried out on WT and R278C$^{+/-}$ hcRTFs, and Ca^{2+}-dependent IAANS fluorescence increase was observed for all hcRTF constructs. The R278C$^{+/-}$ variant showed a statistically significant increase of thin filament Ca^{2+} sensitivity by ~2.3 fold ($p<0.05$) (Figure 2). Stopped-flow fluorescence spectroscopy was used to determine the Ca^{2+} dissociation rates from the hcRTF constructs. Upon the addition of EGTA, the Ca^{2+} rapidly dissociated from cTnC, inducing a cTnC conformational change in which the fluorescence change was recorded. As Ca^{2+} was stripped from cTnC by EGTA, a decrease in IAANS fluorescence was

observed for all hcRTF constructs. hcRTF harboring R278C$^{+/-}$ show a significant decrease of k_{off} compared to WT, significantly increasing the Ca^{2+} sensitivity by ~1.4 fold ($p<0.05$) (Figure 2). This explains, at least in part, the increase of Ca^{2+} sensitivity conferred by the hcRTF harboring the R278C$^{+/-}$ variant in the steady-state experiments.

3.3 Protein quantification and post-translational modification characterization

Previous studies have shown that HCM can largely alter the proteomic profile of the heart, highlighting the extensive underlying pathological remodeling[39,40]. To investigate the proteomic alterations caused by R278C, we obtained the full proteomic profile of *TNNT2* R278C$^{+/-}$ and isogenic control hiPSC-CMs using shotgun, bottom-up mass spectrometry. Here, we found 102 of 2327 proteins to be statistically (1% FDR) more abundant in WT and 198 proteins to be more abundant in R278C$^{+/-}$ cells (Figure 3A). Next, we examined individual proteins of interest involved in control of contractility, structural integrity, metabolism, and crucial cardiac remodeling pathways (Figure 3B-D). The variable profile was further probed among individual protein groups. Even though no significant difference was noted in most sarcomeric proteins, the myosin heavy chain showed a dissimilarity between *TNNT2* R278C$^{+/-}$ and isogenic control hiPSC-CMs. As seen in Figure 3B, the dominant form of myosin heavy chains (MHC), Myosin Heavy chain 7 (MYH7; βMHC) with relatively slow ATPase activity, did not exhibit any quantitative changes between the two groups. However, the other key paralog, MYH6 (αMHC) with relatively fast ATPase activity, was significantly over-expressed in the *TNNT2* R278C$^{+/-}$ hiPSC-CMs. Also, the myosin light chains (MYLs), particularly MYL2, showed a significant decrease in the R278C- harboring CMs relative to the wildtype cells (Figure 3B).

Proteins important for the structural integrity and organization of the Z-disc showed variable translational profiles between the R278C$^{+/-}$ and WT CMs (Figure 3C). α-actinin, a major protein involved in the crosslinking of actin filaments that is disrupted in HCM[41], was significantly increased in *TNNT2* R278C$^{+/-}$ hiPSC-CMs. Meanwhile, other protein groups responsible for the structural integrity and stability of the Z-disc, such as MYOZ2 (Myozenin2), NEBL (Nebulette), and SMPX (small muscle protein)[42,43], were significantly downregulated in R278C$^{+/-}$ hiPSC-CMs, which indicates a further exacerbation of the Z-disc inflexibility and disorganization. Microtubule related proteins such as tubulin β-4B chain (TUBB4B), which play a crucial role in signal transduction and contractility[44], were significantly increased in R278C$^{+/-}$ hiPSC-CMs. Other structural proteins responsible for the overall integrity of the cardiomyocyte also showed significantly lower protein expression in R278C$^{+/-}$ hiPSC-CMs (Figure 3C and D). These include NEBL (Nebulette), which functionally links sarcomeric actin to the desmin intermediate filaments in the sarcomeres[45], JPH2 (Junctophilin2), which provides a structural bridge between the plasma membrane and the sarcoplasmic reticulum and is required for normal excitation- contraction coupling in cardiomyocytes [46], OBSCN (Obscurin), which is involved in the assembly of myosin into sarcomeric A bands [47], FHL 1&2 (Four and a half LIM domains), which negatively regulate the calcineurin/NFAT signaling pathway in cardiomyocytes [38], and DES (Desmin), a key structural intermediate filament required for maintaining normal structure of sarcomeres and

interconnecting the Z-discs[39]. These data suggest significant changes in structural integrity and Z-disc disorganization which may underlie the myofibrillar disarray seen in HCM.

Lastly, a metabolic shift in the proteomic profile was observed in R278C$^{+/-}$ hiPSC-CMs, in which glycolytic proteins were significantly up-regulated, including GLUT1 (insulin-independent glucose transporter protein type 1), PFKAM (ATP-dependent 6-phosphofructokindase muscle type), and PGAM1 (phosphoglycerate mutase 1) (Figure 4A). Meanwhile, major fatty-acid metabolism and β-oxidation proteins, such as ACADS, ACADM, and FABPH, were significantly downregulated in R278C$^{+/-}$ hiPSC-CMs (Figure 4B). These data suggest that R278C may cause a switch to a fetal-like metabolic profile, which has been previously shown in HCM[48]. Additionally, a major metabolic hallmark in HCM is impaired energetics and inefficient ATP utilization[49]. We found CKM (creatine kinase, muscle), CKMT2 (mitochondrial creatine kinase), and ATPD (ATP Synthase F1 Subunit Delta) to be significantly decreased in R278C$^{+/-}$ hiPSC-CMs (Figure 4C), suggesting disrupted cardiac bioenergetics through impaired ATP production and utilization.

In addition to the differences in protein expression, significant alterations were observed on the post translational level, particularly phosphorylation (Figure 5). We found significant dephosphorylation of NFATC2 in *TNNT2* R278C$^{+/-}$ hiPSC-CMs. As the NFAT-Calcineurin pathway is a major contributor to pathological hypertrophy and remodeling[50], this mechanistically links R278C to its potential downstream effects. Moreover, we found MYBPC3 and MYL2, both of which are important regulators of the super relaxed (SRX) and disordered relaxed (DRX) states of the myosin heads[51], to be differentially phosphorylated at sites Ser284 and Ser15, respectively, with higher phosphorylation in R278C$^{+/-}$ hiPSC-CMs. These data suggest a favored transition to the DRX state with R278C, which is a pathological transition seen in HCM.

3.4 Electrophysiological studies in hiPSC-CM monolayers

Using optical mapping on 2D monolayers of R278C$^{+/-}$ and isogenic control hiPSC-CMs, we investigated the effect of various stimulation frequencies on the membrane voltage (Vm) and cytosolic Ca^{2+} transients. Vm and Ca^{2+} transients were determined from the fluorescence emitted by RH-237 and Rhod-2, respectively. Figure 6A shows representative traces of Vm and Ca^{2+} transients from monolayers of hiPSC-CMs electrically stimulated at 55, 65, and 100 beats per minute (bpm). The action potential and Ca^{2+} transients for both control (A1, A2) and R278C$^{+/-}$ (A4, A5) hiPSC-CMs show that both groups entrained normally to 55 and 65 bpm. However, while the control hiPSC-CMs showed normal entrainment to 100 bpm (A3), R278C$^{+/-}$ hiPSC-CMs developed alternans-like irregular and arrhythmogenic voltage and Ca^{2+} transients at this frequency (A6). None of the control hiPSC-CM monolayers exhibited abnormal V_m or Ca^{2+} transients at 100 bpm. This suggests that fast stimulating rates can be arrhythmogenic in R278C$^{+/-}$, which may underlie the higher risk for ventricular arrythmias and sudden death.

We also examined action potential durations at 30% (APD_{30}; B1) and 80% (APD_{80}; B2) of repolarization as a function of stimulation frequency (55, 65, and 75 bpm) in both control and *TNNT2* R278C$^{+/-}$ hiPSC-CMs (Figure 6B). Similarly, we examined Ca^{2+} transient duration at 30% ($CaTD_{30}$; C1) and 80% ($CaTD_{80}$; C2) of repolarization at the same stimulation frequencies (Figure

437 6C). These frequencies were chosen as 55 bpm was higher than the intrinsic beating rate and 75
438 bpm was below frequencies that induced any observable form of arrhythmia. Both APD_{30} and
439 APD_{80} were significantly longer in $R278C^{+/-}$ hiPSC-CMs relative to controls at all frequencies (Figure
440 6B1 and B2). $CaTD_{30}$ was significantly prolonged in $R278C^{+/-}$ hiPSC-CMs compared to WT hiPSC-
441 CM at all stimulation frequencies (Figure 6C1), while $CaTD_{80}$ was significantly prolonged at 65 and
442 75 bpm only (Figure 6C2). Moreover, we found that APD and CaTD significantly shortened with
443 an increase in stimulation frequencies in control hiPSC-CMs, consistent with the concept of
444 restitution. Contrarily, $R278C^{+/-}$ hiPSC-CMs did not exhibit any indication of APD shortening under
445 these experimental conditions, but did, however, display significantly ($p<0.05$) shorter Ca^{2+}
446 transient durations as reflected by reduced $CaTD_{30}$ and $CaTD_{80}$ at 75 vs. 55 bpm. Collectively,
447 $R278C^{+/-}$ disrupts APD and Ca^{2+} transient dynamics, creating electrical instability at higher
448 frequencies.

449 **3.5 $R278C^{+/-}$ demonstrates hypercontractility which is alleviated by mavacamten**

450 Hypercontractility and abnormal sarcomeric shortening are classical features in HCM that drive
451 pathogenesis. To examine the contractile properties of R278C, we employed the newly developed
452 Matlab-based algorithm, SarcTrack, to quantify sarcomeric shortening in α-actinin 2-GFP tagged
453 hiPSC-CMs. The goodness of double wavelet fitting to the sarcomere is shown in Figure 7A.
454 Contractile parameters were measured while the monolayer of hiPSC-CMs was paced at 1 Hz. The
455 percentage of maximal sarcomere shortening was significantly higher in $R278C^{+/-}$ (14.1 ± 0.5%)
456 compared to control (12.8 ± 0.9%) hiPSC-CMs (Figure 7C1). Dramatic increases in the time-to-half
457 maximal contraction and relaxation were also observed in $R278C^{+/-}$ compared to control hiPSC-
458 CMs (Figures 7B1 and C2), which reflected the hypercontractility of $R278C^{+/-}$ variant. However, no
459 significant changes were observed in either the maximum velocity of the relaxation or contraction
460 (Figure 7B2 and C3). We next investigated the effect mavacamten on contraction and relaxation
461 parameters in $R278C^{+/-}$ hiPSC-CMs using various concentrations (0.3, 1, and 3 µM). We found that
462 1 and 3 µM mavacamten caused a significant decrease in the maximum velocity of contraction
463 and the maximum percentage of sarcomere shortening (Figure 8A), and a significant decrease in
464 the maximum velocity of relaxation $R278C^{+/-}$ hiPSC-CMs (Figure 8B). Thus, mavacamten may be a
465 promising therapeutic for HCM patients carrying variants in thin filament proteins such as *TNNT2*
466 $R278C^{+/-}$.

467

468 **4. DISCUSSION**

469 In this study, we generated in *TNNT2* R278C$^{+/-}$ hiPSC-CMs using CRISPR/Cas9 and investigated the
470 pathological consequences of this variant on the proteome and function of hiPSC-CMs
471 Hypercontractility was observed in R278C$^{+/-}$ hiPSC-CMs and mavacamten was found to alleviate
472 it. Furthermore, an increase in Ca^{2+} sensitivity was observed in the R278C$^{+/-}$ hcRTF model.
473 Alterations of AP dynamics and Ca^{2+} handling in R278C$^{+/-}$ CMs were shown to be proarrhythmic
474 at higher stimulation frequencies. Remarkably, the proteome and contractility were dramatically
475 impacted by the insertion of a point mutation in one allele of troponin T and likely has profound
476 consequences in the disease phenotype. Our findings are indicative of potential pathological
477 remodeling in R278C$^{+/-}$ occurring in the early developmental stages of life.

478 **4.1 R278C dynamics and Ca^{2+} sensitivity**

479 Due to the highly flexible nature of cTnT, the molecular structure of most regions of cTnT remain
480 unresolved except for residues 199-272 that are included in the high-resolution troponin core
481 domain crystal structure (PDB: 4Y99)[36] and recently determined thin filament cryo-EM structures
482 (PDB: 6KN7, PDB: 6KN8). The potential energy minimization data for R278C$^{+/-}$ suggests that the
483 cysteine may experience slightly less charge repulsion with nearby residues from actin and Tm.
484 As shown in Figure 1, these nearby residues in actin and tropomyosin create a positively charged
485 microenvironment. We speculate that the charge repulsion between the positively charged native
486 R278 and the local environment might be necessary for its normal function, in which the inherent
487 dynamics and flexibility is required for the molecular movement that is propagated along the thin
488 filament in response to the Ca^{2+} binding to and dissociation from the troponin complex. Previous
489 in vitro functional analyses show that R278C alters Ca^{2+} sensitivity and actin myosin cross-bridging
490 in rabbit, porcine, and human cardiac preparations [17,52–54]. Consistently, our hcRTF models show
491 a similar magnitude of Ca^{2+} sensitization, corroborating the impact of R278C on myofilament
492 dynamics. This is in contrast to studies in R278C$^{+/-}$ transgenic mice, which did not have altered
493 Ca^{2+} sensitivity and did not develop hypertrophy yet displayed diastolic dysfunction[55,56]. This may
494 be explained by the species differences between the mouse and human, particularly for
495 HCM[57],and the experimental models used (skinned cardiomyocytes vs hcRTFs). Further studies
496 are needed to dissect these potential differences.

497 **4.2 Proteomic and post-translational changes**

498 To further emphasize the molecular changes caused by the *TNNT2* R278C$^{+/-}$ variant, we explored
499 the proteomic profile of both cell lines using mass spectrometry. Most species develop many
500 temporally and spatially controlled muscle myosin heavy chain (MYH) paralogs. This implies that
501 diverse MYH paralog features are required for determining contractility qualities. For example,
502 the myosin α heavy chain (MYH6) has fast twitch mechanics response to excitation-contraction
503 coupling, while β-myosin heavy chain (MYH7) has a slower but more powerful stroke[58]. Therefore,
504 the detected increase in MYH6 expression in our study could be a result of increased contractility
505 and cross bridge interactions with the thin filament because of the increased myofilament
506 calcium sensitivity.

507 Myosin light chain-2 (MYL2/MLC-2) is a major sarcomeric protein which is also referred to as the
508 regulatory light chain (RLC) of the contractile unit. MYL2 plays an important role in embryonic
509 heart muscle structure and function, its phosphorylation regulates cardiac myosin cycling kinetics,
510 rotation, and contractility[59]. We found a significant decrease in MYL2 expression levels in R278C$^{+/-}$
511 hiPSC-CMs. This deviation could be attributed to the increased Ca^{2+} sensitivity instigated by the
512 HCM-causing mutations. Hypersensitive myofibrils result in prolonged crossbridge formation,
513 which in turn may result in a disrupted need for regulation by MYL2, leading to a negative
514 response of decreased expression in the variants[60].

515 The presence of mechanical strain on the Z-disc may lead to altered transcriptional regulation
516 through mechanosensitive pathways, affecting the expression profile of several downstream
517 proteins, such as MYH[61,62]. In this study, several alterations were found to be directly or indirectly
518 associated with Z-disc disorganization and myofibrillar disarray. For instance, α-actinin is a major
519 protein found in the Z-disc and is involved in the crosslinking of actin filaments. In HCM, α-actinin
520 is expected to increase due to the greater mechanical stiffness of the CM[42]. Microtubules also
521 play a crucial role in signal transduction and contractility. There is a growing interest in exploring
522 the role of microtubules in affecting diastolic compliance[63]. The upregulation of tubulin β-4B
523 chain in our study could be indicative of elevated tubulin polymerization and stabilization, which
524 is an early pathological adaptive response in cardiomyopathies and heart failure that can induce
525 stiffness which directly affects the diastolic compliance of the cell.

526 Our results suggest that R278C$^{+/-}$ hiPSC-CMs undergo a switch to a fetal metabolic program, as
527 demonstrated by high expression of glucose genes and lower expression of fatty acid metabolism
528 proteins. The switch to a fetal metabolic profile is commonly seen in HCM and heart failure and
529 may initially be an adaptive response[49]. We additionally found protein changes suggestive of
530 impaired bioenergetics and ATP synthesis or utilization. Impaired sarcomere energetics in HCM
531 may provoke mitochondrial dysfunction, reduced ATP production, and increased reactive oxygen
532 species (ROS) generation. All these indices are directly related to a potential pathogenic decline
533 in the rate of the electron transport chain, leading to lower amounts of respiratory complex
534 proteins[49,64]. Our findings both coincide with and differ from those found by Gilda e*t al* in a 3-
535 month-old transgenic mouse model in which R278C overexpression caused increased AMP levels
536 indicating metabolic stress yet also decreased glycolysis related proteins[65]. Therefore, the impact
537 of species and age on impaired bioenergetics in HCM needs to be further investigated.

538 Cardiac contractility is regulated by numerous factors including the phosphorylation of
539 sarcomeric proteins. In relaxed heart muscle there is evidence for a population of myosin cross-
540 bridges with the two heads in an interacting motif (IHM) that establish a so-called super relaxed
541 state (SRX) with low ATPase activity that is sequestered from interacting with the thin filaments.
542 Another population of cross-bridges exists in a disordered relaxed (DRX) state with swaying free
543 heads poised to interact with the thin filaments, hydrolyze ATP, and induce force generation and
544 shortening with calcium activation. In healthy and relaxed human hearts, it is proposed that most
545 myosin heads exist in the SRX state but in pathological conditions like HCM, the IHM state of

546 myosin is disturbed and the percentage of DRX is increased. Phosphorylation of myosin binding
547 protein-C (MyBPC3) and myosin regulatory light chain (MYL2) may promote the DRX state by
548 recruitment of sequestered IHM heads [51]. Our study provides evidence for the favored transition
549 to the DRX state, in which an increased number of phosphorylated peptides exist in MYBPC3 and
550 MYL2 at sites Ser284 and Ser15, respectively. Sarcomere shortening velocity may also be further
551 affected with the increased phosphorylation of MYBPC3 at Ser284. In a transgenic mouse model,
552 MYBPC3 phosphorylation was found to change both filament orientation and mechanics of
553 contractility by modulation of the SRX state, although no direct effect was observed on Ca^{2+}
554 sensitivity[66]. Additionally, the substitution of arginine (R) with a cysteine (C) in R278C introduces
555 a novel residue for a possible S-glutathionylation. Future studies will explore the modifications on
556 the C278 residue, particularly, S-glutathionylation, which can modulate sarcomeric proteins
557 involved in contraction in relation to changes in the oxidative state of the cell[67].

558 **4.3 Electrophysiological and contractile abnormalities**

559 Tachycardia in HCM patients carrying *TNNT2* variants can be arrhythmogenic. In this regard, the
560 rapid heart rate resulted in atrial fibrillation or sinus tachycardia in over 90% of the arrhythmic
561 episodes in HCM patients who were recipients of implantable cardiac defibrillators (ICDs)[68].
562 Moreover, sinus tachycardia was observed in 90% of ventricular fibrillation episodes in HCM
563 affected children who were treated with heart rate therapeutics. The results of these studies are
564 consistent with the high incidence of ventricular tachycardia and sudden cardiac arrest possibly
565 linked to high Ca^{2+} sensitivity due to cTnT mutations[5,12,17]. Our results in R278C$^{+/-}$ hiPSC-CMs
566 demonstrate that fast stimulating rates can be arrhythmogenic compared to control *TNNT2* hiPSC-
567 CMs. Although the mechanisms of arrhythmogenesis are not clear, alterations in Ca^{2+}-handling
568 properties are likely involved. Increased Ca^{2+} sensitivity due to cTnT variants has been previously
569 shown to increase cytosolic Ca^{2+} buffering, since the troponin complex accounts for a substantial
570 portion of cytosolic Ca^{2+} buffering[69,70]. During diastole, increased Ca^{2+} sensitivity results in the
571 prolongation of Ca^{2+} transient and slower Ca^{2+} decay rate. In previous studies[71,72], a theory for the
572 mechanism of intracellular Ca^{2+} alternans was developed. It is called the "3R" theory since Ca^{2+}
573 alternans is promoted by the interactions of random firing of the Ca^{2+} sparks, recruitment of
574 neighboring Ca^{2+} release units (CRUs) for firing (spark-induced sparks), and refractoriness of the
575 CRUs. The recruitment is determined by the coupling strength between CRUs, and Ca^{2+} buffering
576 is one of the parameters affecting recruitment[73]. In this mechanism, Ca^{2+} alternans are promoted
577 by the enhancement of the recruitment[72]. This theory may explain the Ca^{2+} alternans observed
578 in our study. Increased thin filament Ca^{2+} sensitivity appears to be primarily due to the decrease
579 in the Ca^{2+} off rate constant. This reduction/slow-down of the unbinding rate of Ca^{2+} from the
580 myofilament effectively can reduce Ca^{2+} buffering, which can promote Ca^{2+}alternans based on the
581 "3R" theory[71–73].

582 Moreover, we found the R278C$^{+/-}$ variant to enhance contractility. These findings may be related
583 to the prolonged Ca^{2+} transients seen in R278C$^{+/-}$ hiPSC-CMs. Based on the proteomic results, a
584 reduction in the SRX myosin due to the MYBCP3 and MYL2 phosphorylation may also be regarded
585 as a possible mechanism for increased contractility in R278C$^{+/-}$ hiPSC-CMs[66]. Interestingly,

586 mavacamten was able to alleviate hypercontractility in R278C$^{+/-}$, which may owe to its ability to
587 reduce the number of myosin heads available to interact with actin by promoting the SRX state,
588 which is thought to improve diastolic dysfunction in HCM[74]. Our results are consistent with
589 previous studies examining mavacamten hiPSC-CM models of HCM[74,75]. Thus, mavacamten may
590 be a promising treatment for thin filament HCM that should be investigated further.

591 **4.4 Clinical pathogenicity of *TNNT2* R278C**

592 Like many cardiomyopathy-associated genetic variants, the clinical pathogenicity of the *TNNT2*
593 R278C variant in HCM is controversial. Given that it is now reported in over 50 patients carrying
594 a diagnosis of HCM, it is of critical importance to better understand its role in disease. ClinVar, a
595 publicly accessible online database of human disease associated genetic variants, currently
596 reports conflicting interpretations of pathogenicity[8]. Select laboratories and research groups have
597 reported it to be pathogenic/likely pathogenic, while others have downgraded it to a variant of
598 uncertain significance in HCM (Supplementary Table S1). A major reason to question its
599 association with a relatively uncommon human disease is its higher frequency in the general
600 population (0.06%), as reported in the Genome Aggregation Database (gnomAD)[76]. However,
601 *TNNT2* R278C is generally associated with a late onset of milder HCM, and a relatively higher
602 allele frequency in the general population may be consistent with a low penetrance, high
603 frequency disease-causing variant[77], as has been described in other forms of genetic
604 cardiomyopathy[78,79]. Additionally, thin filament (e.g., *TNNT2*) HCM expresses differently than
605 classic thick filament HCM, often causing diastolic heart failure and arrhythmias with borderline
606 ventricular hypertrophy. This makes it more difficult to detect on imaging, particularly in the
607 presence of hypertension and aortic valvular disease, which are prevalent in both the general and
608 late-onset HCM populations (i.e., age 50 or older).

609 Several studies have reported additional variants in *MYH7* or *MYBPC3* in HCM individuals with
610 the R278C variant. Although this has brought into question whether R278C is in itself pathogenic,
611 it is important to note that HCM cases have been reported without the presence of additional
612 variants, and not all of the additional variants identified are definitively or likely pathogenic. As
613 described in ClinVar (Supplementary Table S1), 14 out of 47 R278C$^{+/-}$ carriers who had HCM
614 possessed an additional variant, which were in MYH7 or MYBPC3. Of these, only 4 out of the 14
615 possessed a confirmed pathogenic/likely pathogenic secondary variant. Moreover, evidence of
616 co-segregation exists even in families without secondary variants, although expressivity of the
617 R278C variant is incomplete[9,11,12,15]. Therefore, the capability of R278C to result in disease does
618 not seem dependent on the presence of a secondary HCM-associated variant. However, the co-
619 occurrence of HCM-associated variants can affect expressivity and phenotype severity by acting
620 synergistically to accentuate disease manifestation[80]. For instance, Gimeno *et al.* reported that
621 R278C carriers which carried a pathogenic/likely pathogenic secondary variant in MYH7
622 (p.Asp928Asn) presented with a severe HCM phenotype[81]. Moreover, the presence of an
623 additional variant may not be the only explanation for incomplete expressivity in R278C carriers.
624 The ratio of mutant to wild-type protein expression levels and the impact of post-translational
625 modifications may also contribute. Schuldt et al observed a dose-dependent relationship

626 between the mutant R278C protein expression dose and myofilament function in detergent-
627 extracted cardiomyocytes from the interventricular septum of *TNNT2* R278C$^{+/-}$ patients using
628 troponin exchange experiments. The *TNNT2* R278C$^{+/-}$ variant showed increased Ca^{2+} sensitivity at
629 low doses and a significant increase at intermediate doses[54]. Altogether, our hiPSC-CM study
630 supports the pathogenicity of *TNNT2* R278C$^{+/-}$, although follow up studies are required to address
631 the incomplete penetrance and whether R278C acts as a disease modifier in the presence of
632 secondary variants in thick filament proteins.

633 **4.5 Limitations**

634 This study aimed to uncover the proteomic and functional alterations in the early stages of
635 R278C$^{+/-}$ HCM using various approaches. Despite that, several limitations arose that could be
636 improved in future experiments. Firstly, the protein purification protocol is based on a magnetic
637 bead-based solvation layer that captures mostly hydrophilic proteins or soluble portions of
638 proteins. This presents a limitation in studying hydrophobic or membrane-bound proteins (e.g.,
639 ion channels). Secondly, functional studies were conducted with only hiPSC-derived
640 cardiomyocytes in 2D monolayers, which could be improved with 3D tissue that includes
641 fibroblasts and endothelial cells, which contribute to the clinical phenotype. Lastly, we did not
642 study the impact of maturation on disease severity, which has been shown to accentuate HCM in
643 hiPSC-CMs studies[82].

644 **4.6 Conclusions**

645 We show that R278C increases Ca^{2+} sensitivity, alters APD and Ca^{2+} transient dynamics, causes
646 hypercontractility, largely disrupts the proteome, and may promote NFAT signaling and a
647 transition towards greater of myosin head in the DRX state. These insights improve our
648 understanding of thin filament HCM and may be transformative for clinical diagnosis and
649 management.

650

651 **Author contributions**:

652 SS Experimental: genome editing ; hiPSC differentiation ; optical mapping
653 AYL Experimental: recombinant protein expression, reconstituted cardiac thin filaments
654 FJ Experimental: hiPSC differentiation, hiPSC-CM protein extraction, MS proteomics
655 YM Experimental: hiPSC differentiation; SarcTrack analyses
656 SD Clinical expertise in familial HCM, ClinVar analysis, manuscript writing
657 HH Expertise in hiPSC-CM maturation
658 DHB Expertise in microtubules
659 TB Experimental: genome editing
660 BR Experimental: genome editing
661 SJ Experimental: PDMS matrix design and fabrication
662 TR Clinical expertise in familial HCM
663 AC Experimental: Potential energy minimization simulations of the cardiac thin filament
664 PL Data analysis – thin filament expertise
665 RJS troponin structure and function expertise
666 SS Clinical expertise in familial HCM
667 CT SarcTrack expertise
668 SL Potential energy minimization simulations of the cardiac thin filament
669 PL MS proteomics expertise
670 GFT PI on project, grant holder, project designer and coordinator
671

672 **Competing interests**.
673 R.J.S. is a member of the Scientific Advisor Board of Cytokinetics, Inc., and a consultant to
674 Myokardia/Bristol- Myers-Squibb.
675

676 **Acknowledgements**
677 The authors are very grateful for the funding supporting this work from several granting agencies.
678 This includes the National Institutes of Health (R01HL137015) to SL, (HLBI RO1 HL158634-01A1)
679 to RJS, Stem Cell Network (FY21 / ACCT2-13) to GFT, and the Canadian Institutes of Health
680 Research (PJT 185981) to GFT. Members of the Cellular and Regenerative Medicine Centre at the
681 BC Children's Hospital Research Institute are thoroughly indebted to the BC Children's Hospital
682 Foundation and the Mining for Miracles teams for their incredible infrastructural support.
683

684 **REFERENCES**

685 1. Maron BJ, Towbin JA, Thiene G, Antzelevitch C, Corrado D, Arnett D, Moss AJ, Seidman CE,
686 Young JB. Contemporary definitions and classification of the cardiomyopathies: An
687 American Heart Association Scientific Statement from the Council on Clinical Cardiology,
688 Heart Failure and Transplantation Committee; Quality of Care and Outcomes Research and
689 Functional Genomics and Translational Biology Interdisciplinary Working Groups; and
690 Council on Epidemiology and Prevention. *Circulation* 2006;**113**:1807–1816.
691 2. Elliott PM, Poloniecki J, Dickie S, Sharma S, Monserrat L, Varnava A, Mahon NG, Mckenna
692 WJ. Hypertrophic Cardiomyopathy Sudden Death in Hypertrophic Cardiomyopathy:
693 Identification of High Risk Patients. *Journal of the American College of Cardiology*.
694 3. Maron, B. J. *et al.* Contemporary Definitions and Classification of the
695 Cardiomyopathies. *Circulation* **113**, 1807–1816 (2006).
696 4. Varnava AM, Elliott PM, Baboonian C, Davison F, Davies MJ, McKenna WJ. Hypertrophic
697 Cardiomyopathy Histopathological Features of Sudden Death in Cardiac Troponin T
698 Disease. *Circulation* **12**, 1380-4 (2001).
699 5. Driest SL Van, Ellsworth EG, Ommen SR, Tajik AJ, Gersh BJ, Ackerman MJ. Prevalence and
700 spectrum of thin filament mutations in an outpatient referral population with hypertrophic
701 cardiomyopathy. *Circulation* 2003;**108**:445–451.
702 6. Marian AJ, Roberts R. The molecular genetic basis for hypertrophic cardiomyopathy.
703 *Journal of Molecular and Cellular Cardiology*. Academic Press; 2001. p655–670.
704 7. Tadros HJ, Life CS, Garcia G, Pirozzi E, Jones EG, Datta S, Parvatiyar MS, Chase PB, Allen HD,
705 Kim JJ, Pinto JR, Landstrom AP. Meta-analysis of cardiomyopathy-associated variants in
706 troponin genes identifies loci and intragenic hot spots that are associated with worse
707 clinical outcomes. *J Mol Cell Cardiol* 2020;**142**:118–125.
708 8. National Center for Biotechnology Information. ClinVar; [VCV000012411.58],
709 https://www.ncbi.nlm.nih.gov/clinvar/variation/VCV000012411.58 (accessed Aug. 6,
710 2023)
711 9. Alfares AA, Kelly MA, McDermott G, Funke BH, Lebo MS, Baxter SB, Shen J, McLaughlin HM,
712 Clark EH, Babb LJ, Cox SW, Depalma SR, Ho CY, Seidman JG, Seidman CE, Rehm HL. Results
713 of clinical genetic testing of 2,912 probands with hypertrophic cardiomyopathy: Expanded
714 panels offer limited additional sensitivity. *Genetics in Medicine* 2015;**17**:880–888.
715 10. Miliou A, Anastasakis A, D'Cruz LG, Theopistou A, Rigopoulos A, Rizos I, Stamatelopoulos S,
716 Toutouzas P, Stefanadis C. Low prevalence of cardiac troponin T mutations in a Greek
717 hypertrophic cardiomyopathy cohort. *Heart* 2005;**91**:966–967.
718 11. Theopistou A, Anastasakis A, Miliou A, Rigopoulos A, Toutouzas P, Stefanadis C. Clinical
719 features of hypertrophic cardiomyopathy caused by an Arg278Cys missense mutation in
720 the cardiac troponin T gene. *American Journal of Cardiology* 2004;**94**:246–249.
721 12. Watkins, H. *et al.* Mutations in the genes for cardiac troponin T and alpha-tropomyosin in
722 hypertrophic cardiomyopathy. *N Engl J Med* **332**, 1058–1064 (1995).

723 13. Kaski JP, Syrris P, Esteban MTT, Jenkins S, Pantazis A, Deanfield JE, McKenna WJ, Elliott PM.
724 Prevalence of sarcomere protein gene mutations in preadolescent children with
725 hypertrophic cardiomyopathy. *Circ Cardiovasc Genet* 2009;**2**:436–441.
726 14. Gruner C, Care M, Siminovitch K, Moravsky G, Wigle ED, Woo A, Rakowski H. Sarcomere
727 protein gene mutations in patients with apical hypertrophic cardiomyopathy. *Circ*
728 *Cardiovasc Genet* 2011;**4**:288–295.
729 15. Brito D, Miltenberger-Miltenyi G, Pereira SV, Silva D, Diogo AN, Madeira H. Sarcomeric
730 hypertrophie cardiomyopathy: Genetic profile in a Portuguese population. *Revista*
731 *Portuguesa de Cardiologia* 2012;**31**:577–587.
732 16. Tester DJ, Ackerman MJ. Cardiomyopathic and channelopathic causes of sudden
733 unexplained death in infants and children. *Annu Rev Med* **60**, 69–84 (2009).
734 17. Knollmann BC, Potter JD. Altered regulation of cardiac muscle contraction by troponin T
735 mutations that cause familial hypertrophic cardiomyopathy. *Trends Cardiovasc Med* **11**,
736 206– 212 (2001).
737 18. Eschenhagen, T., Mummery, C. & Knollmann, B. C. Modelling sarcomeric cardiomyopathies
738 in the dish: from human heart samples to iPSC cardiomyocytes. *Cardiovasc Res* **105**, 424–
739 438 (2015).
740 19. Pettinato AM, Ladha FA, Mellert DJ, Legere N, Cohn R, Romano R, Thakar K, Chen YS, Hinson
741 JT. Development of a Cardiac Sarcomere Functional Genomics Platform to Enable Scalable
742 Interrogation of Human TNNT2 Variants. *Circulation* 2020;**142**:2262–2275.
743 20. Shafaattalab S, Li AY, Gunawan MG, Kim BR, Jayousi F, Maaref Y, Song Z, Weiss JN, Solaro
744 RJ, Qu Z, Tibbits GF. Mechanisms of Arrhythmogenicity of Hypertrophic Cardiomyopathy-
745 Associated Troponin T (TNNT2) Variant I79N. *Front Cell Dev Biol* 2021;**9**.
746 21. Erdmann J, Daehmlow S, Wischke S, Senyuva M, Werner U, Raible J, Tanis N, Dyachenko S,
747 Hummel M, Hetzer R, Regitz-Zagrosek V. Mutation spectrum in a large cohort of unrelated
748 consecutive patients with hypertrophic cardiomyopathy. *Clin Genet* 2003;**64**:339–349.
749 22. Toepfer CN, Sharma A, Cicconet M, Garfinkel AC, Mücke M, Neyazi M, Willcox JAL, Agarwal
750 R, Schmid M, Rao J, Ewoldt J, Pourquié O, Chopra A, Chen CS, Seidman JG, Seidman CE.
751 SarcTrack. *Circ Res* 2019;**124**:1172–1183.
752 23. Yamada Y, Namba K, Fujii T. Cardiac muscle thin filament structures reveal calcium
753 regulatory mechanism. *Nat Commun* 2020;**11**.
754 24. Alford RF, Leaver-Fay A, Jeliazkov JR, O'Meara MJ, DiMaio FP, Park H, Shapovalov M V.,
755 Renfrew PD, Mulligan VK, Kappel K, Labonte JW, Pacella MS, Bonneau R, Bradley P,
756 Dunbrack RL, Das R, Baker D, Kuhlman B, Kortemme T, Gray JJ. The Rosetta All-Atom Energy
757 Function for Macromolecular Modeling and Design. *J Chem Theory Comput* 2017;**13**:3031–
758 3048.
759 25. Wang C, Bradley P, Baker D. Protein-Protein Docking with Backbone Flexibility. *J Mol Biol*
760 2007;**373**:503–519.
761 26. Coulton A, Lehrer SS, Geeves MA. Functional homodimers and heterodimers of
762 recombinant smooth muscle tropomyosin. *Biochemistry* 2006;**45**:12853–12858.

763 27. Shafaattalab S, Li AY, Lin E, Stevens CM, Dewar LJ, Lynn FC, Sanatani S, Laksman Z, Morin
764 RD, Petegem F van, Hove-Madsen L, Peter Tieleman D, Davis JP, Tibbits GF. In vitro analyses
765 of suspected arrhythmogenic thin filament variants as a cause of sudden cardiac death in
766 infants. *Proc Natl Acad Sci U S A* 2019;**116**:6969–6974.
767 28. Davis JP, Norman C, Kobayashi T, Solaro RJ, Swartz DR, Tikunova SB. Effects of thin and thick
768 filament proteins on calcium binding and exchange with cardiac troponin C. *Biophys J*
769 2007;**92**:3195–3206.
770 29. Ran FA, Hsu PD, Wright J, Agarwala V, Scott DA, Zhang F. Genome engineering using the
771 CRISPR-Cas9 system. *Nat Protoc* 2013;**8**:2281–2308.
772 30. Richardson CD, Ray GJ, DeWitt MA, Curie GL, Corn JE. Enhancing homology-directed
773 genome editing by catalytically active and inactive CRISPR-Cas9 using asymmetric donor
774 DNA. *Nat Biotechnol* 2016;**34**:339–344.
775 31. Hughes CS, Moggridge S, Müller T, Sorensen PH, Morin GB, Krijgsveld J. Single-pot, solid-
776 phase-enhanced sample preparation for proteomics experiments. *Nat Protoc* 2019;**14**:68–
777 85.
778 32. Gunawan MG, Sangha SS, Shafaattalab S, Lin E, Heims-Waldron DA, Bezzerides VJ, Laksman
779 Z, Tibbits GF. Drug screening platform using human induced pluripotent stem cell-derived
780 atrial cardiomyocytes and optical mapping. *Stem Cells Transl Med* 2021;**10**:68–82.
781 33. Shafaattalab S, Lin E, Christidi E, Huang H, Nartiss Y, Garcia A, Lee J, Protze S, Keller G,
782 Brunham L, Tibbits GF, Laksman Z. Ibrutinib Displays Atrial-Specific Toxicity in Human Stem
783 Cell-Derived Cardiomyocytes. *Stem Cell Reports* 2019;**12**:996–1006.
784 34. Kovács M, Tóth J, Hetényi C, Málnási-Csizmadia A, Seller JR. Mechanism of blebbistatin
785 inhibition of myosin II. *Journal of Biological Chemistry* 2004;**279**:35557–35563.
786 35. Baudenbacher F, Schober T, Pinto JR, Sidorov VY, Hilliard F, Solaro RJ, Potter JD, Knollmann
787 BC. Myofilament Ca2+ sensitization causes susceptibility to cardiac arrhythmia in mice.
788 *Journal of Clinical Investigation* 2008;**118**:3893–3903.
789 36. Marston S, Zamora JE. Troponin structure and function: a view of recent progress. *J Muscle*
790 *Res Cell Motil* 2020;**41**:71–89.
791 37. Takeda S, Yamashita A, Maeda K, Maéda Y. Structure of the core domain of human
792 cardiac troponin in the Ca(2+)-saturated form. *Nature* **424**, 35–41 (2003).
793 38. Marian AJ. Molecular Genetic Basis of Hypertrophic Cardiomyopathy. *Circ Res*
794 2021;**128**:1533–1553.
795 39. Coats CJ, Heywood WE, Virasami A, Ashrafi N, Syrris P, Remedios C Dos, Treibel TA, Moon
796 JC, Lopes LR, McGregor CGA, Ashworth M, Sebire NJ, McKenna WJ, Mills K, Elliott PM.
797 Proteomic Analysis of the Myocardium in Hypertrophic Obstructive Cardiomyopathy. *Circ*
798 *Genom Precis Med* 2018;**11**:e001974.
799 40. Previs MJ, O'Leary TS, Morley MP, Palmer BM, Lewinter M, Yob JM, Pagani FD, Petucci C,
800 Kim MS, Margulies KB, Arany Z, Kelly DP, Day SM. Defects in the Proteome and Metabolome
801 in Human Hypertrophic Cardiomyopathy. *Circ Heart Fail* 2022;**15**:E009521.
802 41. Girolami F, Iascone M, Tomberli B, Bardi S, Benelli M, Marseglia G, Pescucci C, Pezzoli L,
803 Sana ME, Basso C, Marziliano N, Merlini PA, Fornaro A, Cecchi F, Torricelli F, Olivotto I. Novel

α-actinin 2 variant associated with familial hypertrophic cardiomyopathy and juvenile atrial arrhythmias: A massively parallel sequencing study. *Circ Cardiovasc Genet* 2014;**7**:741–750.

42. Wadmore K, Azad AJ, Gehmlich K. The Role of Z-disc Proteins in Myopathy and Cardiomyopathy. *Int J Mol Sci* **22**, 3058 (2021).
43. Wang H, Li Z, Wang J, Sun K, Cui Q, Song L, Zou Y, Wang X, Liu X, Hui R, Fan Y. Mutations in NEXN, a Z-Disc gene, are associated with hypertrophic cardiomyopathy. *Am J Hum Genet* 2010;**87**:687–693.
44. Caporizzo, M. A., Chen, C. Y., Bedi, K., Margulies, K. B. & Prosser, B. L. Microtubules Increase Diastolic Stiffness in Failing Human Cardiomyocytes and Myocardium. *Circulation* **141**, 902– 915 (2020).
45. Perrot A, Tomasov P, Villard E, Faludi R, Melacini P, Lossie J, Lohmann N, Richard P, Bortoli M De, Angelini A, Varga-Szemes A, Sperling SR, Simor T, Veselka J, Özcelik C, Charron P. Mutations in NEBL encoding the cardiac Z-disk protein nebulette are associated with various cardiomyopathies. *Archives of Medical Science* 2016;**12**:263–278.
46. Beavers DL., Landstrom AP, Chiang DY, Wehrens XHT. Emerging roles of junctophilin-2 in the heart and implications for cardiac diseases. *Cardiovascular Research* **103**, 198–205 (2014).
47. Marston, S. Obscurin variants and inherited cardiomyopathies. *Biophys Rev* **9**, 239–243 (2017).
48. Velden J Van Der, Tocchetti CG, Varricchi G, Bianco A, Sequeira V, Hilfiker-Kleiner D, Hamdani N, Leite-Moreira AF, Mayr M, Falcao-Pires I, Thum T, Dawson DK, Balligand JL, Heymans S. Metabolic changes in hypertrophic cardiomyopathies: Scientific update from the working group of myocardial function of the European Society of Cardiology. *Cardiovascular Research* **10**, 1273-1280 (2018).
49. Ranjbarvaziri S, Kooiker KB, Ellenberger M, Fajardo G, Zhao M, Roest AS Vander, Woldeyes RA, Koyano TT, Fong R, Ma N, Tian L, Traber GM, Chan F, Perrino J, Reddy S, Chiu W, Wu JC, Woo JY, Ruppel KM, Spudich JA, Snyder MP, Contrepois K, Bernstein D. Altered Cardiac Energetics and Mitochondrial Dysfunction in Hypertrophic Cardiomyopathy. *Circulation* 2021;**144**:1714–1731.
50. Wilkins BJ, Dai YS, Bueno OF, Parsons SA, Xu J, Plank DM, Jones F, Kimball TR, Molkentin JD. Calcineurin/NFAT Coupling Participates in Pathological, but not Physiological, Cardiac Hypertrophy. *Circ Res* 2004;**94**:110–118.
51. Schmid M, & Toepfer CN, Cardiac myosin super relaxation (SRX): a perspective on fundamental biology, human disease and therapeutics. *Biology Open* **10**, bio057646 (2021).
52. Yanaga F, Morimoto S, Ohtsuki I. Ca2+ Sensitization and Potentiation of the Maximum Level of Myofibrillar ATPase Activity Caused by Mutations of Troponin T Found in Familial Hypertrophic Cardiomyopathy. *J Biol Chem* **13**, 8806-12 (1999).

843 53. Morimoto S, Nakaura H, Yanaga F, Ohtsuki I. Functional Consequences of a Carboxyl
844 Terminal Missense Mutation Arg278Cys in Human Cardiac Troponin T. *Biochem Biophys Res*
845 *Commun.* **1,** 79-82 (1999).
846 54. Schuldt M, Johnston JR, He H, Huurman R, Pei J, Harakalova M, Poggesi C, Michels M, Kuster
847 DWD, Pinto JR, Velden J van der. Mutation location of HCM-causing troponin T mutations
848 defines the degree of myofilament dysfunction in human cardiomyocytes. *J Mol Cell*
849 *Cardiol* 2021;**150**:77–90.
850 55. Hernandez OM, Szczesna-Cordary D, Knollmann BC, Miller T, Bell M, Zhao J, Sirenko SG,
851 Diaz Z, Guzman G, Xu Y, Wang Y, Kerrick WGL, Potter JD. F110I and R278C troponin T
852 mutations that cause familial hypertrophic cardiomyopathy affect muscle contraction in
853 transgenic mice and reconstituted human cardiac fibers. *Journal of Biological Chemistry*
854 2005;**280**:37183–37194.
855 56. Sirenko SG, Potter JD, Knollmann BC. Differential effect of troponin T mutations on the
856 inotropic responsiveness of mouse hearts - Role of myofilament Ca2+ sensitivity increase.
857 *Journal of Physiology* 2006;**575**:201–213.
858 57. Vakrou S, Liu Y, Zhu L, Greenland G V., Simsek B, Hebl VB, Guan Y, Woldemichael K, Talbot
859 CC, Aon MA, Fukunaga R, Abraham MR. Differences in molecular phenotype in mouse and
860 human hypertrophic cardiomyopathy. *Sci Rep* 2021;**11**.
861 58. Walklate J, Ferrantini C, Johnson CA, Tesi C, Poggesi C, Geeves MA. Alpha and beta myosin
862 isoforms and human atrial and ventricular contraction. *Cell. Mol. Life Sci.* **78**, 7309–7337
863 (2021).
864 59. Sheikh F, Lyon RC, Chen J. Functions of myosin light chain-2 (MYL2) in cardiac muscle and
865 disease. *Gene* **569**, 14–20 (2015).
866 60. Markandran K, Poh JW, Ferenczi MA, Cheung C. Regulatory light chains in cardiac
867 development and disease. *Int J Mol Sci* **22**, 4351 (2021).
868 61. Rysä J, Tokola H, Ruskoaho H. Mechanical stretch induced transcriptomic profiles in cardiac
869 myocytes. *Sci Rep* 2018;**8**.
870 62. Lyon RC, Zanella F, Omens JH, Sheikh F. Mechanotransduction in cardiac hypertrophy and
871 failure. *Circ Res* **116**, 1462–1476 (2015).
872 63. Caporizzo MA, Chen CY, Bedi K, Margulies KB, Prosser BL. Microtubules Increase Diastolic
873 Stiffness in Failing Human Cardiomyocytes and Myocardium. *Circulation* 2020;**141**:902–
874 915.
875 64. Vakrou S, Abraham MR. Hypertrophic cardiomyopathy: A heart in need of an energy bar?
876 *Frontiers in Physiology* **5**, (2014).
877 65. Gilda JE, Lai X, Witzmann FA, Gomes A V. Delineation of molecular pathways involved in
878 cardiomyopathies caused by Troponin T Mutations. *Molecular and Cellular Proteomics*
879 2016;**15**:1962–1981.
880 66. Sadayappan S, Gulick J, Osinska H, Martin LA, Hahn HS, Dorn GW, Klevitsky R, Seidman CE,
881 Seidman JG, Robbins J. Cardiac myosin-binding protein-C phosphorylation and cardiac
882 function. *Circ Res* 2005;**97**:1156–1163.

883 67. Rosas PC, Solaro RJ. Implications of S-glutathionylation of sarcomere proteins in cardiac
884 disorders, therapies, and diagnosis. *Frontiers in Cardiovascular Medicine* **9**, (2023).
885 68. Kaski JP, Esteban MTT, Lowe M, Sporton S, Rees P, Deanfield JE, McKenna WJ, Elliott PM.
886 Outcomes after implantable cardioverter-defibrillator treatment in children with
887 hypertrophic cardiomyopathy. *Heart* 2007;**93**:372–374.
888 69. Miller T, Szczesna D, Housmans PR, Zhao J, Freitas F De, Gomes A V., Culbreath L, McCue J,
889 Wang Y, Xu Y, Kerrick WGL, Potter JD. Abnormal Contractile Function in Transgenic Mice
890 Expressing a Familial Hypertrophic Cardiomyopathy-linked Troponin T (I79N) Mutation.
891 *Journal of Biological Chemistry* 2001;**276**:3743–3755.
892 70. Calcium Fluxes Involved in Control of Cardiac Myocyte Contraction. *Circ Res* **87**, 275– 281
893 (2000).
894 71. Qu Z, Liu MB, Nivala M. A unified theory of calcium alternans in ventricular myocytes. *Sci*
895 *Rep* 2016;**6**.
896 72. Rovetti R, Cui X, Garfinkel A, Weiss JN, Qu Z. Spark-induced sparks as a mechanism of
897 intracellular calcium alternans in cardiac myocytes. *Circ Res* 2010;**106**:1582–1591.
898 73. Nivala M, Lange E de, Rovetti R, Qu Z. Computational modeling and numerical methods for
899 spatiotemporal calcium cycling in ventricular myocytes. *Frontiers in Physiology* **3**, (2012).
900 74. Sewanan LR, Shen S, Campbell SG. Mavacamten preserves length-dependent contractility
901 and improves diastolic function in human engineered heart tissue. *Am J Physiol Heart Circ*
902 *Physiol* 2021;**320**:H1112–H1123.
903 75. Bhagwan JR, Mosqueira D, Chairez-Cantu K, Mannhardt I, Bodbin SE, Bakar M, Smith JGW,
904 Denning C. Isogenic models of hypertrophic cardiomyopathy unveil differential phenotypes
905 and mechanism-driven therapeutics. *J Mol Cell Cardiol* 2020;**145**:43–53.
906 76. Karczewski KJ, Francioli LC, Tiao G, Cummings BB, Alföldi J, Wang Q, Collins RL, Laricchia
907 KM, Ganna A, Birnbaum DP, Gauthier LD, Brand H, Solomonson M, Watts NA, Rhodes D,
908 Singer-Berk M, England EM, Seaby EG, Kosmicki JA, Walters RK, Tashman K, Farjoun Y, Banks
909 E, Poterba T, Wang A, Seed C, Whiffin N, Chong JX, Samocha KE, Pierce-Hoffman E, Zappala
910 Z, O'Donnell-Luria AH, Minikel EV, Weisburd B, Lek M, Ware JS, Vittal C, Armean IM,
911 Bergelson L, Cibulskis K, Connolly KM, Covarrubias M, Donnelly S, Ferriera S, Gabriel S,
912 Gentry J, Gupta N, Jeandet T, Kaplan D, Llanwarne C, Munshi R, Novod S, Petrillo N, Roazen
913 D, Ruano-Rubio V, Saltzman A, Schleicher M, Soto J, Tibbetts K, Tolonen C, Wade G,
914 Talkowski ME, Aguilar Salinas CA, Ahmad T, Albert CM, Ardissino D, Atzmon G, Barnard J,
915 Beaugerie L, Benjamin EJ, Boehnke M, Bonnycastle LL, Bottinger EP, Bowden DW, Bown MJ,
916 Chambers JC, Chan JC, Chasman D, Cho J, Chung MK, Cohen B, Correa A, Dabelea D, Daly
917 MJ, Darbar D, Duggirala R, Dupuis J, Ellinor PT, Elosua R, Erdmann J, Esko T, Färkkilä M,
918 Florez J, Franke A, Getz G, Glaser B, Glatt SJ, Goldstein D, Gonzalez C, Groop L, Haiman C,
919 Hanis C, Harms M, Hiltunen M, Holi MM, Hultman CM, Kallela M, Kaprio J, Kathiresan S,
920 Kim BJ, Kim YJ, Kirov G, Kooner J, Koskinen S, Krumholz HM, Kugathasan S, Kwak SH, Laakso
921 M, Lehtimäki T, Loos RJF, Lubitz SA, Ma RCW, MacArthur DG, Marrugat J, Mattila KM,
922 McCarroll S, McCarthy MI, McGovern D, McPherson R, Meigs JB, Melander O, Metspalu A,
923 Neale BM, Nilsson PM, O'Donovan MC, Ongur D, Orozco L, Owen MJ, Palmer CNA, Palotie

A, Park KS, Pato C, Pulver AE, Rahman N, Remes AM, Rioux JD, Ripatti S, Roden DM, Saleheen D, Salomaa V, Samani NJ, Scharf J, Schunkert H, Shoemaker MB, Sklar P, Soininen H, Sokol H, Spector T, Sullivan PF, Suvisaari J, Tai ES, Teo YY, Tiinamaija T, Tsuang M, Turner D, Tusie-Luna T, Vartiainen E, Watkins H, Weersma RK, Wessman M, Wilson JG, Xavier RJ, Daly MJ. The mutational constraint spectrum quantified from variation in 141,456 humans. *Nature* 2020;**581**:434–443.

77. P M Elliott, L D'Cruz, W J McKenna. Late-onset hypertrophic cardiomyopathy caused by a mutation in the cardiac troponin T gene. *N Engl J Med.* **24**, (1999).

78. Akinrinade O, Koskenvuo JW, Alastalo TP. Prevalence of titin truncating variants in general population. *PLoS One* 2015;**10**.

79. Maestro-Benedicto A, Vela P, Frutos F de, Mora N, Pomares A, Gonzalez-Vioque E, Briceño A, Cabrera E, Cobo-Marcos M, Dominguez F, Gonzalez-Lopez E, Segovia J, Lara-Pezzi E, Garcia-Pavia P. Frequency of hereditary transthyretin amyloidosis among elderly patients with transthyretin cardiomyopathy. *Eur J Heart Fail* 2022;**24**:2367–2373.

80. Burns C, Bagnall RD, Lam L, Semsarian C, Ingles J. Multiple Gene Variants in Hypertrophic Cardiomyopathy in the Era of Next-Generation Sequencing. *Circ Cardiovasc Genet* 2017;**10**.

81. Gimeno JR, Tomé-Esteban M, Lofiego C, Hurtado J, Pantazis A, Mist B, Lambiase P, McKenna WJ, Elliott PM. Exercise-induced ventricular arrhythmias and risk of sudden cardiac death in patients with hypertrophic cardiomyopathy. *Eur Heart J* 2009;**30**:2599–2605.

82. Knight WE, Cao Y, Lin YH, Chi C, Bai B, Sparagna GC, Zhao Y, Du Y, Londono P, Reisz JA, Brown BC, Taylor MRG, Ambardekar A V., Cleveland JC, McKinsey TA, Jeong MY, Walker LA, Woulfe KC, D'Alessandro A, Chatfield KC, Xu H, Bristow MR, Buttrick PM, Song K. Maturation of Pluripotent Stem Cell-Derived Cardiomyocytes Enables Modeling of Human Hypertrophic Cardiomyopathy. *Stem Cell Reports* 2021;**16**:519–533.

949 **FIGURE CAPTIONS**

950 **Figure 1. Computational modelling and potential energy minimization.** Panels A. and B. show
951 troponin T (cyan), actin chain F (brown), tropomyosin chain W (green), and tropomyosin chain X
952 (purple). Panel A. shows the structure of the complex with WT troponin T (with residue R278).
953 Panel B. includes the predicted structure of the complex with the genetic variant R278C$^{+/-}$.
954 Residues with side chain atoms displayed correspond to the five closest residues that the R278
955 CG (γ carbon) atom and C278 SG (γ sulfur) atom have in common. Panels C. and D. show troponin
956 T (cyan) and the surfaces of actin chain F and tropomyosin chain W. The surfaces of these chains
957 are colored with respect to their Coulombic surface potential, where blue indicates positive
958 residues, red indicates negative residues, and white corresponds to neutral residues. Panel C.
959 shows the structure of the complex with R278, and Panel D. shows the modelled structure of the
960 Tn complex that harbors the mutant residue C278. Labels shown are in the format: one letter
961 residue code, residue number, chain ID.

962 **Figure 2. Steady-state and stopped-flow analysis of Ca^{2+} kinetics in human cardiac reconstituted**
963 **thin filaments (hcRTF).** Panel A. The Ca^{2+} sensitivity (expressed in K_d (μM)) of the WT and R278C$^{+/-}$
964 hcRTF was determined by steady-state fluorescence spectrometry. The R278C significantly
965 decreased the K_d compared to the WT counterpart by ~2-fold, indicating that this variant
966 increases the Ca^{2+} sensitivity significantly in the hcRTF biochemical system. Panel B. A stopped-
967 flow instrument was used to determine the Ca^{2+} dissociation rates (expressed in k_{off} (s^{-1})) from
968 the hcRTF. Upon the addition of EGTA, the Ca^{2+} was rapidly removed from TnC, inducing a
969 conformational change in cTnC within hcRTF in which the fluorescence change was recorded. The
970 R278C$^{+/-}$ hcRTF exhibited a decrease in the k_{off} by ~1.5 fold, compared to the WT counterpart,
971 suggesting that the increase in Ca^{2+} sensitivity observed in the steady state is largely due to a
972 slower Ca^{2+} off-loading rate. *p<0.05, **p<0.05, ***p<0.005.

973 **Figure 3. MS proteomic abundance profiles.** Panel A. Volcano plot comparison of WT vs. R278C$^{+/-}$
974 on the protein expression levels. The right side of the plot (red) reflects upregulated proteins in
975 R278C$^{+/-}$ hiPSC-CMs, and the left side (black) shows the proteins that were detected in higher
976 quantity in the WT hiPSC-CMs. The FDR threshold was set to 0.01, and any data points beyond
977 that were considered as statistically significant. Gene ontology (GO) annotation terms summarize
978 the top cross search results in reference to KEGG, Elsevier, Jensen, and GO biological processes
979 databases. Panels B-D. Violin plot representations of individual proteins that exhibited significant
980 changes between the R278C$^{+/-}$ vs. WT and separated according to their functional groups. Panel
981 B. Thick filament proteins: MYH7 (myosin heavy chain-7), MYH6 (myosin heavy chain-6), MYL2
982 (myosin regulatory light chain ventricular isoform), and MYL6 (myosin regulatory light chain-6).
983 Panel C. Z-disc proteins: ACTN1 (Alpha actinin-1), MYOZ2 (Myozenin-2), NEBL (Nebulette),
984 PDLIM5 (PDZ and LIM domain protein-5), SMPX (Small muscular protein), and CSRP3 (Cysteine
985 and glycine-rich protein-3). Panel D. Cardiac remodelling proteins: DESM (Desmin), JPH2
986 (Junctophilin-2), IQGAP1 (Ras GTPase-activating- like protein), OBSCN (Obscurin), FHL1 (Four and

987 a half LIM domains protein-1), and FHL2 (Four and a half LIM domains protein-2). *p<0.05,
988 **p<0.05, ***p<0.005; two-tailed unpaired t-test.

989 **Figure 4. MS proteomic abundance profile of metabolic and energy production proteins**. Panel
990 A. PGAM1 (Phosphoglycerate mutase-1), PFKAM (ATP-dependent 6- phosphofructokinase,
991 muscle type), GLUT1 (Solute carrier family 2, facilitated glucose transporter member-1). Panel B.
992 ACADM (Medium-chain specific acyl-CoA dehydrogenase), ACADS (Short-chain specific acyl- CoA
993 dehydrogenase), FABPH (Fatty acid binding protein, heart). Panel C. CKM (Creatine kinase M-
994 type), CKMT2 (Creatine kinase mitochondrial type 2), and ATPD (ATP synthase subunit delta,
995 mitochondrial). (* p-value< 0.05, ** p-value <0.005, ***p-value<0.0005; two-tailed unpaired t-
996 test.)

997 **Figure 5. Phosphorylation profile of six selected phosphosites in R278C$^{+/-}$ vs. WT hiPSC-CMs**.
998 Dot plot representation of the phosphorylation change relative to the total protein expression.
999 The degree of WT phosphorylation was used as the baseline to compare the phosphorylation
1000 trends in the chosen phosphosites in the R278C$^{+/-}$ hiPSC-CMs.

1001 **Figure 6. Optical mapping (OM) of membrane voltage (Vm) and calcium (Ca^{2+}) transients in 2D**
1002 **monolayers of hiPSC-CMs**. Panel A. Representative OM traces of V_m (red) and Ca^{2+} (black)
1003 transients in WT (A1 to A3) and R278C$^{+/-}$ (A4 to A6) hiPSC-CMs at three different stimulation
1004 frequencies 55, 65, 100 bpm in the top, middle, and bottom traces, respectively. WT hiPSCs
1005 responded normally to all stimulation frequencies, however, about 50% of R278C$^{+/-}$ hiPSC-CMs
1006 exhibited voltage and Ca^{2+} alternans at frequencies above 75 bpm. Panel B. Statistical analysis of
1007 action potential duration of WT (black) and R278C$^{+/-}$ (red) hiPSC-CMs as a function of stimulation
1008 frequencies over the range of 55 to 75 BPM. Panels B1 and B2 show that both the APD_{30} and
1009 APD_{80} were significantly longer in R278C$^{+/-}$ vs. WT at all stimulation frequencies. Panel C1 shows
1010 that the $CaTD_{30}$ was significantly longer in R278C$^{+/-}$ vs. WT at all stimulation frequencies. Panel C2
1011 exhibits the longer $CaTD_{80}$ in R278C$^{+/-}$ vs WT hiPSCs at 65 and 75 bpm. (* p-value< 0.05, ** p-
1012 value <0.005, ***p-value<0.0005)

1013 **Figure 7. SarcTrack analysis of WT and R278C$^{+/-}$ hiPSC-CM contractile properties**. Panel A. GFP-
1014 tagged α-actinin hiPSC-CMs cultured on 5 kPa PDMS (left) and SarcTrack wavelet fitting (right).
1015 Panel B. The relaxation of WT (black, n=9) and R278C$^{+/-}$ (red, n=12) hiPSC-CMs cultured on 5 kPa
1016 PDMS, with respect to: B1) time-to-half maximal relaxation (ms). B2) the maximum velocity of
1017 relaxation ($\mu m \cdot s^{-1}$). Panel C. The contractile parameters of WT (black, n=9) and R278C$^{+/-}$ (red,
1018 n=12) hiPSC-CMs cultured on 5 kPa PDMS and stimulated at 1 Hz with respect to: C1) percent
1019 maximal shortening; C2) time to half maximal contraction; C3) maximum velocity of contraction
1020 ($\mu m\ s^{-1}$). (* p-value< 0.05, ** p-value <0.005, ***p-value<0.0005)

1021 **Figure 8. SarcTrack analysis of the effect of mavacamten on** R278C$^{+/-}$ **hiPSC-CM contractile**
1022 **properties**. Panel A. The effect of mavacamten on the contractile parameters of R278C$^{+/-}$ (red,
1023 n=37) hiPSC-CMs cultured on 5 kPa PDMS and stimulated at 1 Hz with respect to: A1) maximum
1024 velocity of contraction ($\mu m.\ s^{-1}$) and A2) percent maximal shortening. Panel B. The effect of

1025 mavacamten on the relaxation of R278C$^{+/-}$ (red, n=37) hiPSC-CMs cultured on 5 kPa PDMS, with
1026 respect to the maximum velocity of relaxation (µm. s-1). (* p-value< 0.05, ** p-value <0.005,
1027 ***p-value<0.0005)

1028 **Figure S1. Phylogenetic sequence alignment of cardiac troponin T (TNNT2)**. A multiple species
1029 sequence alignment of the cTnT protein (encoded by *TNNT2*) from human (Uniprot ID: P45379),
1030 bovine (Uniprot ID: P13789), rabbit (Uniprot ID: P09741), rat (Uniprot ID: P50753), mouse
1031 (Uniprot ID: P50752), chicken (Uniprot ID: P02642), and zebrafish (Uniprot ID: Q90Y46) was
1032 performed using Clustal Omega. The equivalent residue R278 among all species are boxed in red
1033 and is shown to be highly conserved.

1034 **Figure S2. Genome Editing to Generate TNNT2 R278C$^{+/-}$ and WT hiPSC-CMs**. Panel A. Schematic
1035 of CRISPR/Cas9 design strategies to target R278 in *TNNT2* (R288 prior to postnatal Exon 5
1036 alternative splicing) in two different hiPSC lines iPS(IMR900)-4 (sgRNA 1, ssODN 1, teal) and AICS-
1037 0075 cl.87 (sgRNA 2, ssODN 2, orange). The sequence shows the C>T mutation locus for R278C
1038 (highlighted in yellow). Panel B. Representative chromatograms of exon 16 in *TNNT2* from isolated
1039 iPS(IMR900)-4 (top) and AICS-0075 cl.87 (bottom) lines showing the heterozygous C>T base pair
1040 change as double-peaks post-editing for R278C. The C>A silent PAM site mutation is also shown
1041 in Design 2. The figure was created using Benchling and SnapGene software. WT = wild-type;
1042 hiPSC = human induced pluripotent stem cells; sgRNA = single guide RNA; ssODN = single-
1043 stranded oligonucleotide.

Table 1: Average intensity of the slow skeletal (*TNNI1*) and the cardiac (*TNNI3*) troponin 1 paralogs.

Average intensity	***WT***	***R278C***
TNNI1	32.41	31.75
TNNI3	24.69	25.34
TNNI3/TNNI1	0.76	0.80

Figure 1

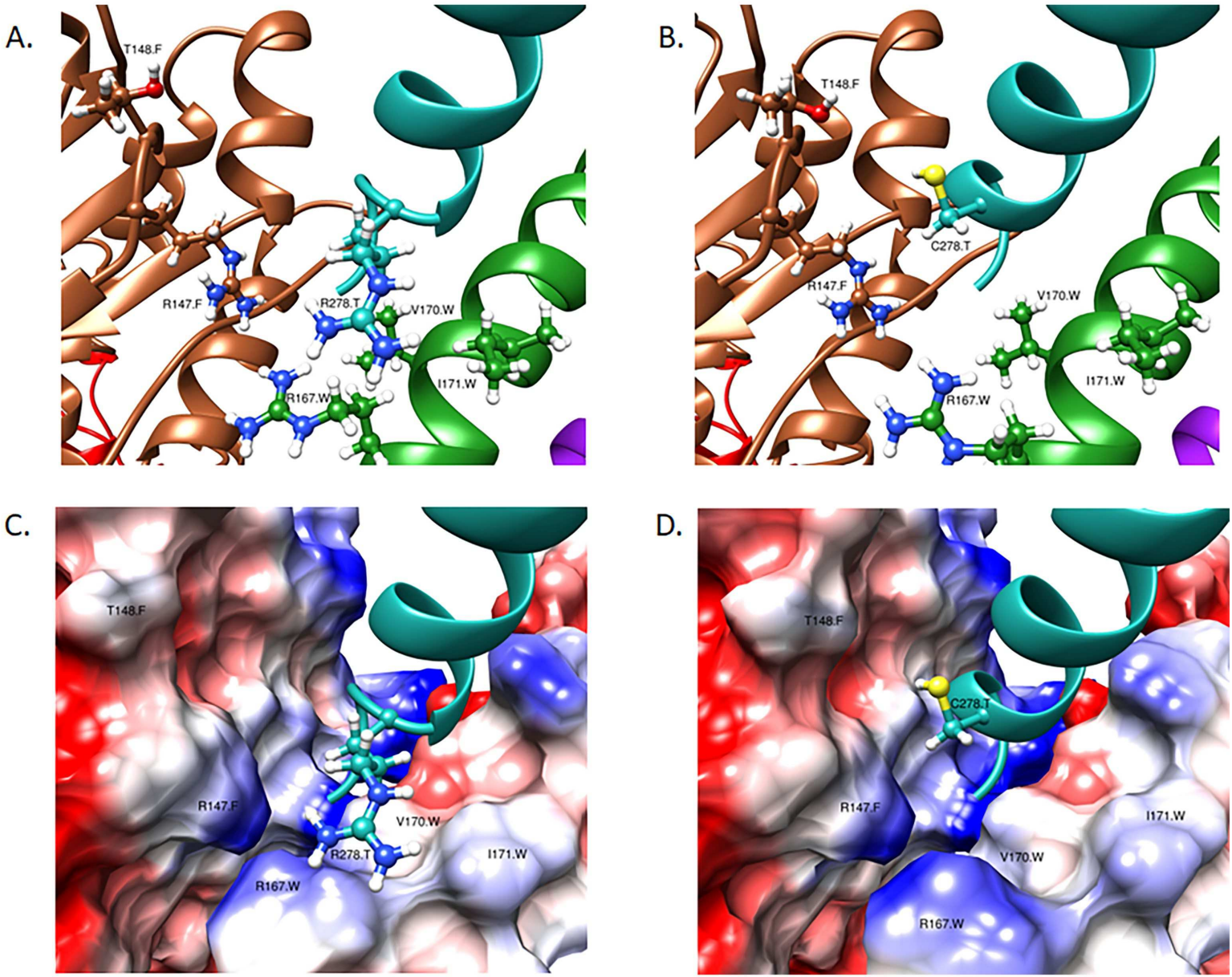
A.
T148.F
R147.F
R278.T
V170.W
I171.W
R167.W
B.
T148.F
C278.T
R147.F
V170.W
I171.W
R167.W
C.
T148.F
R147.F
V170.W
R278.T
I171.W
R167.W
D.
T148.F
C278.T
R147.F
I171.W
V170.W
R167.W

Figure 2

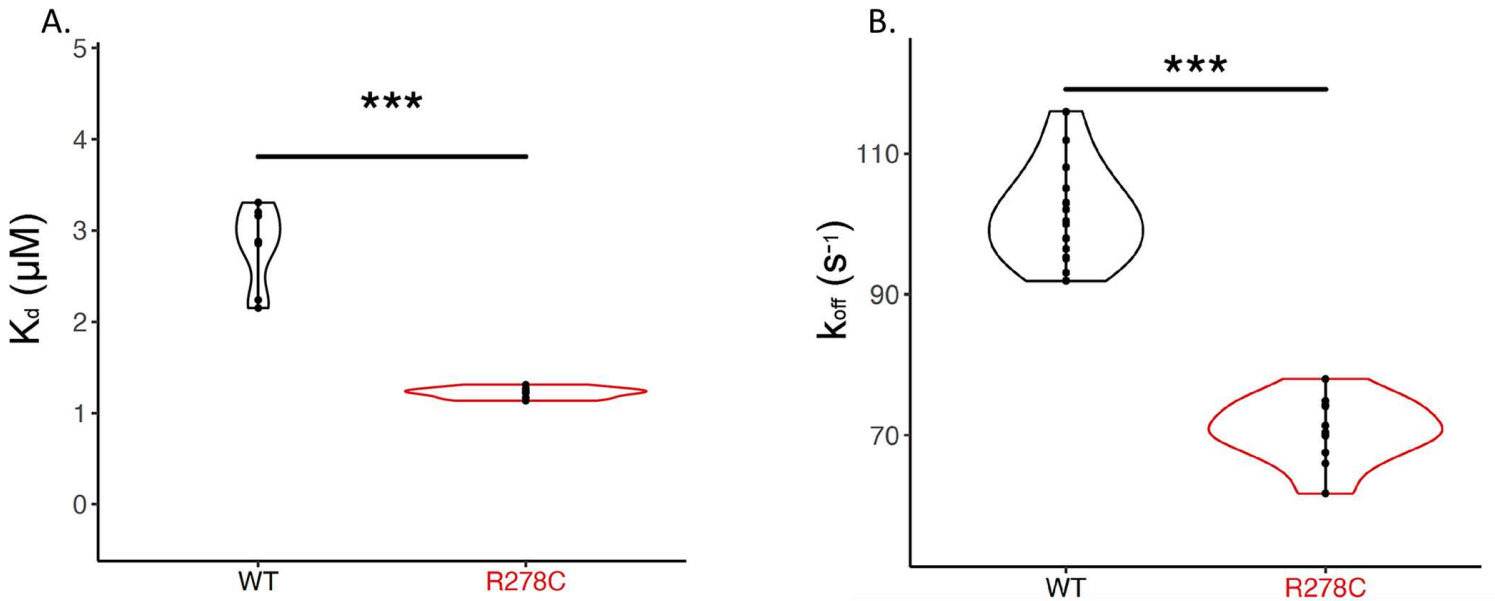

Figure 3

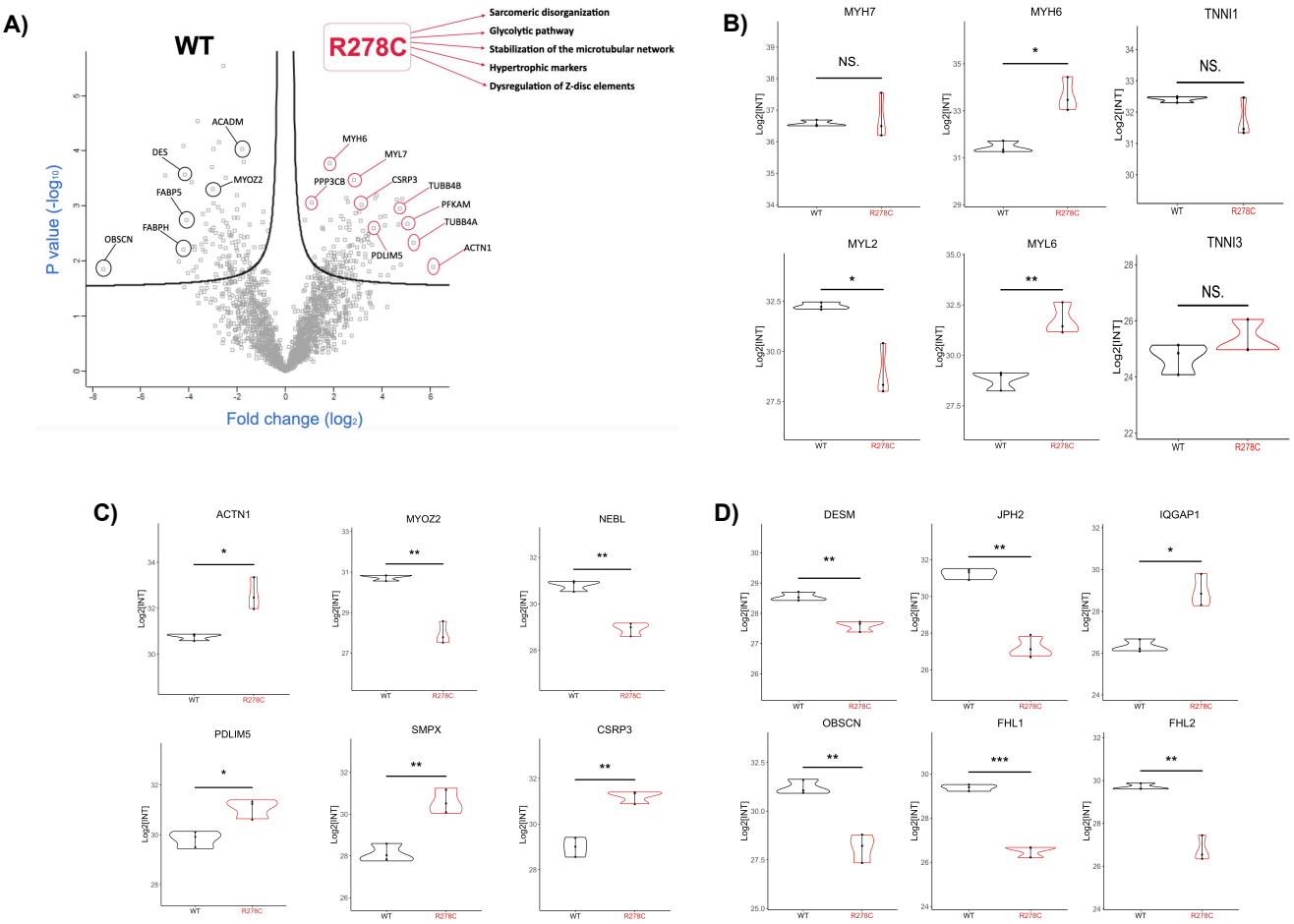
A)
WT
R278C
Sarcomeric disorganization
Glycolytic pathway
Stabilization of the microtubular network
Hypertrophic markers
Dysregulation of Z-disc elements
ACADM
DES
MYOZ2
FABP5
FABPH
OBSCN
MYH6
MYL7
PPP3CB
CSRP3
TUBB4B
PFKAM
TUBB4A
PDLIM5
ACTN1
P value (-log10)
Fold change (log2)
B)
MYH7
MYH6
TNNI1
MYL2
MYL6
TNNI3
NS.
Log2[INT]
WT
R278C
C)
ACTN1
MYOZ2
NEBL
PDLIM5
SMPX
CSRP3
D)
DESM
JPH2
IQGAP1
OBSCN
FHL1
FHL2

Figure 4

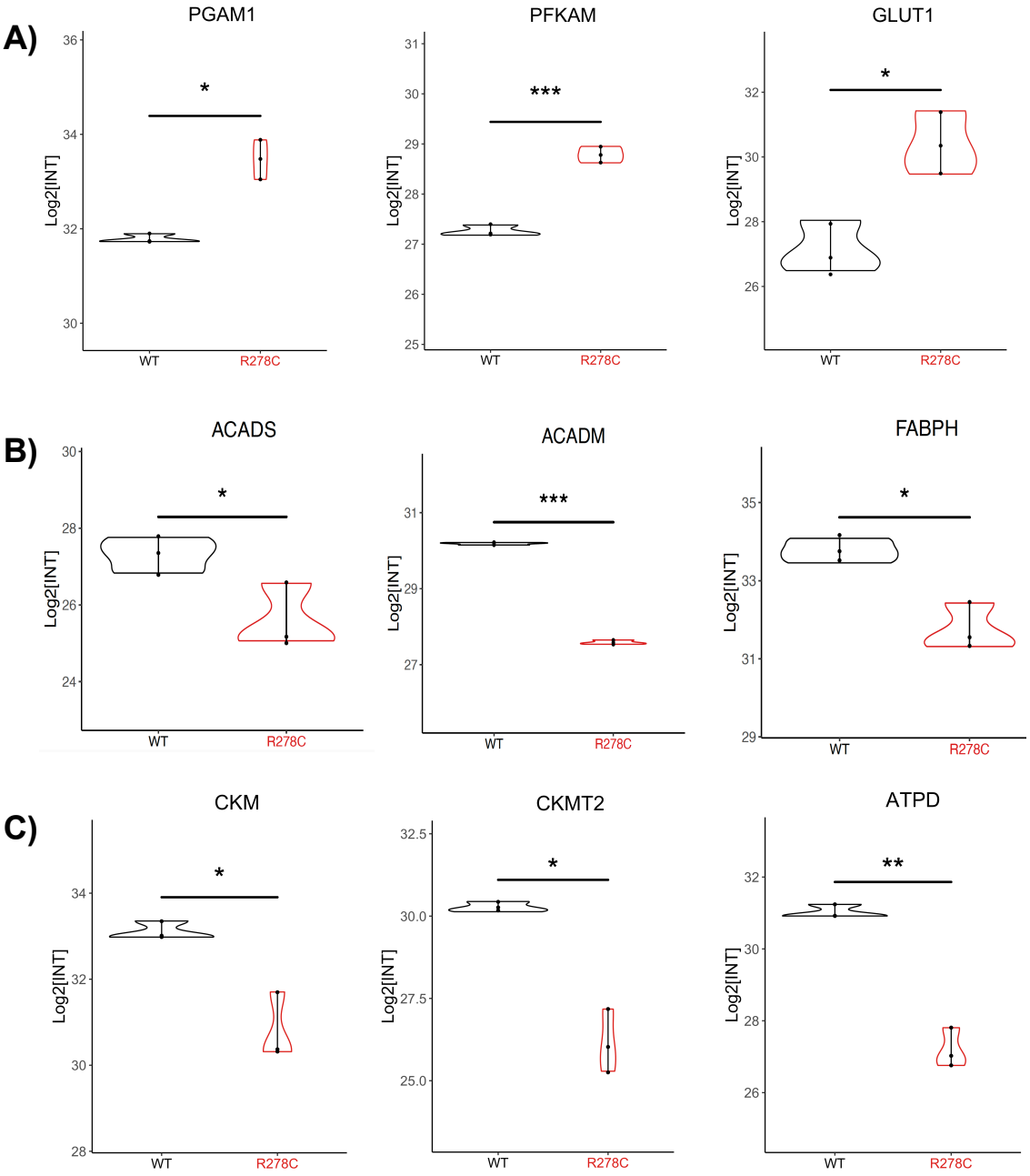
A)
PGAM1
PFKAM
GLUT1
B)
ACADS
ACADM
FABPH
C)
CKM
CKMT2
ATPD
Log2[INT]
WT
R278C
*
***
**

Figure 5

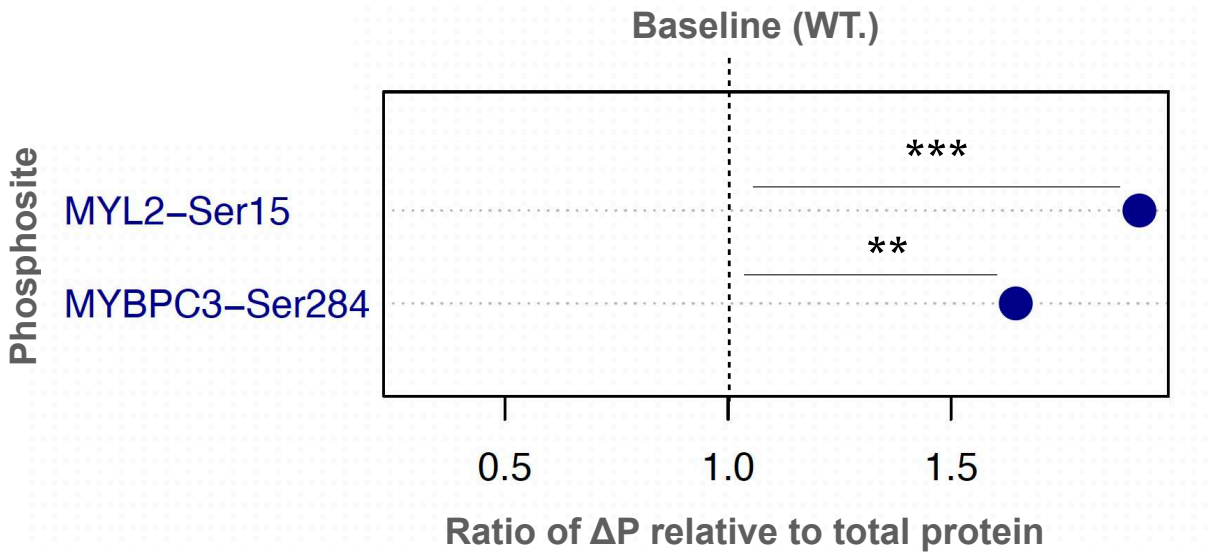
Baseline (WT.)
Phosphosite
MYL2–Ser15
MYBPC3–Ser284
***
**
0.5
1.0
1.5
Ratio of ΔP relative to total protein

Figure 6

A. Representative voltage and Ca^{2+} transients

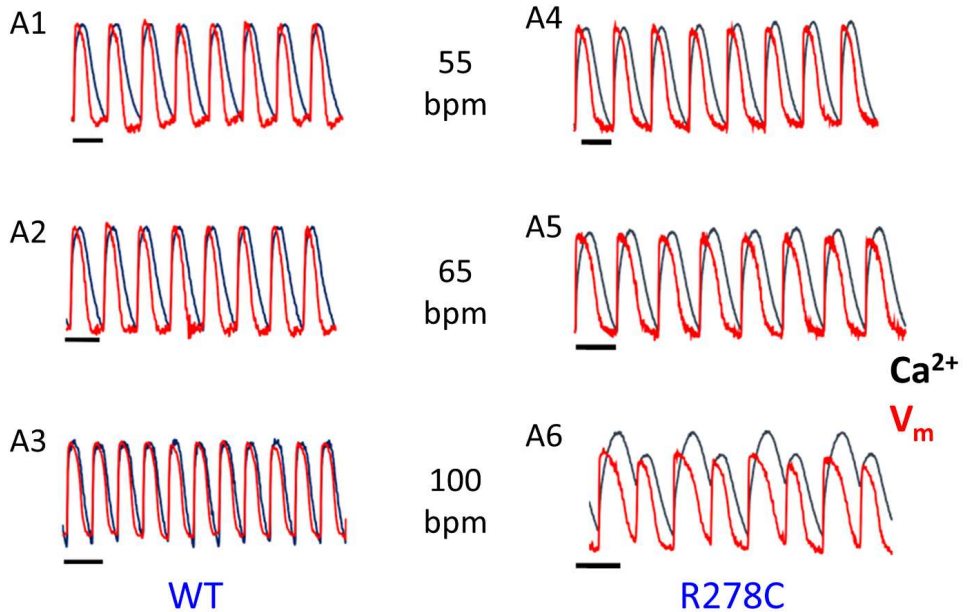

B. Action potential duration

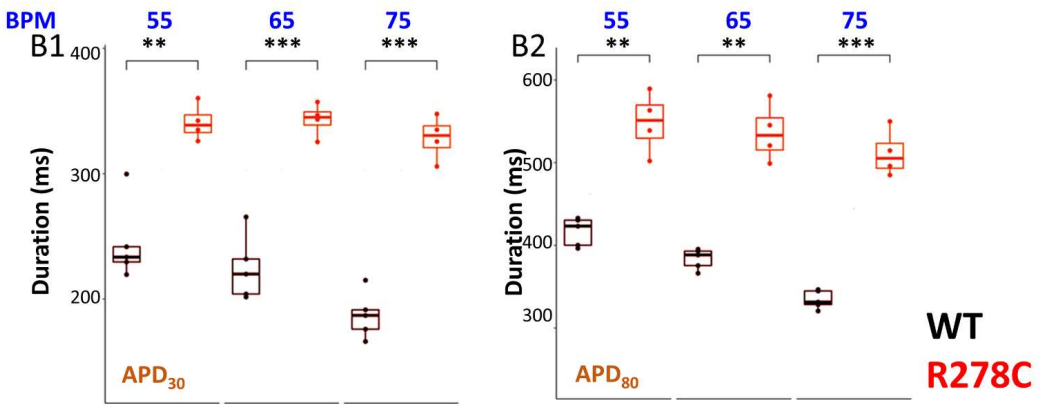

C. Ca^{2+} transient duration

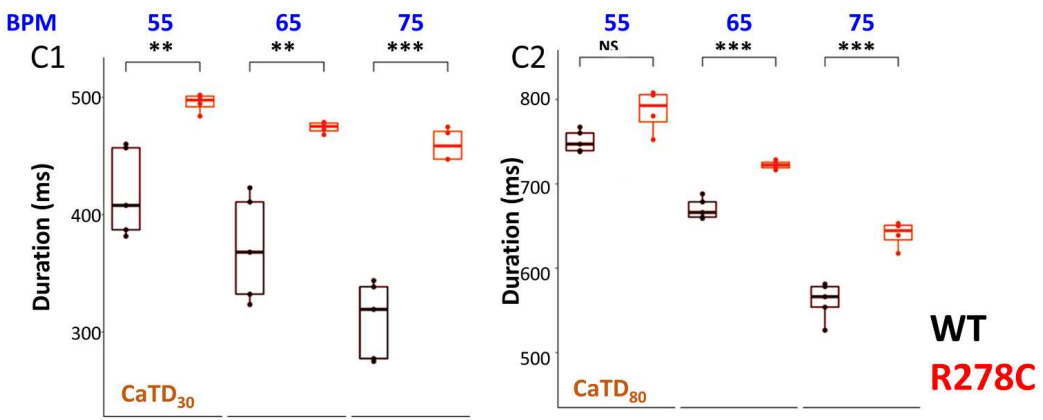

Figure 7

A.

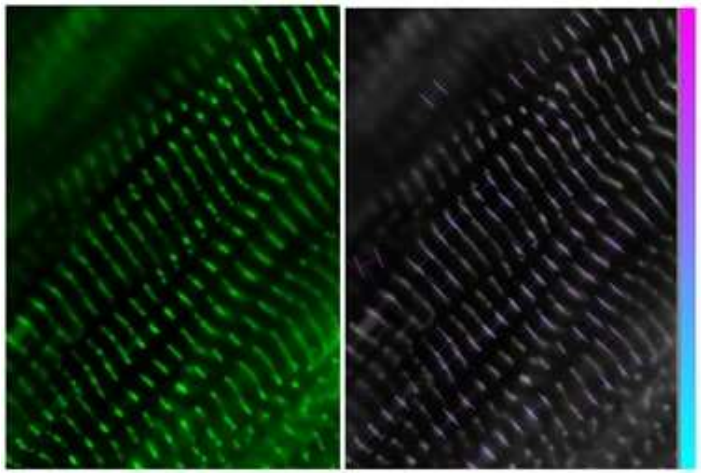

B.

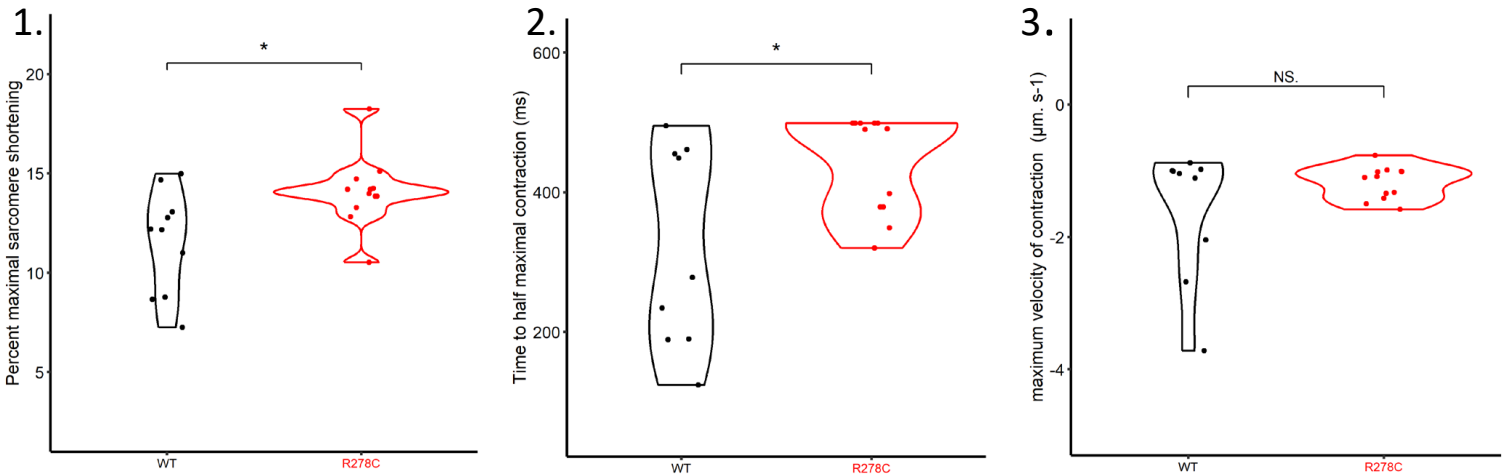
1.
Percent maximal sarcomere shortening
20
15
10
5
*
WT
R278C
2.
Time to half maximal contraction (ms)
600
400
200
*
WT
R278C
3.
maximum velocity of contraction (µm. s-1)
0
-2
-4
NS.
WT
R278C

C.

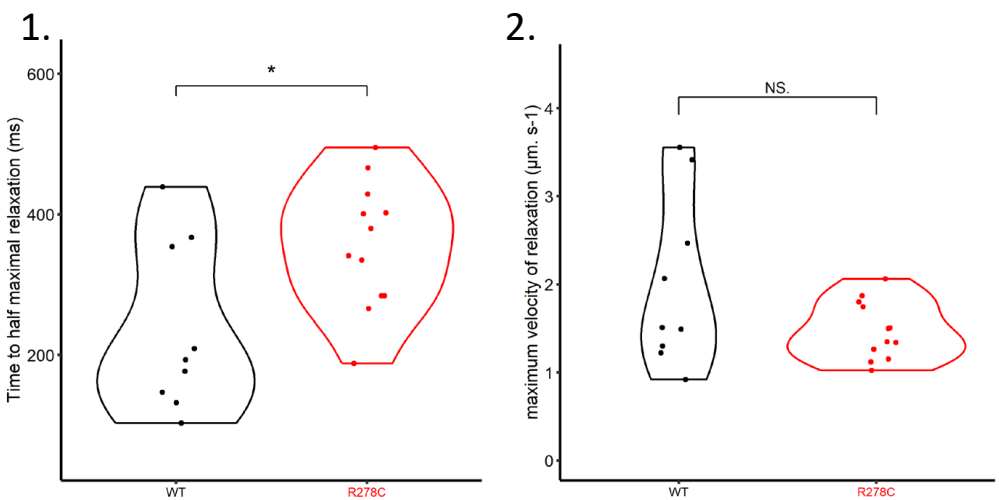
1.
Time to half maximal relaxation (ms)
600
400
200
*
WT
R278C
2.
maximum velocity of relaxation (µm. s-1)
4
3
2
1
0
NS.
WT
R278C

Figure 8

A.

1.

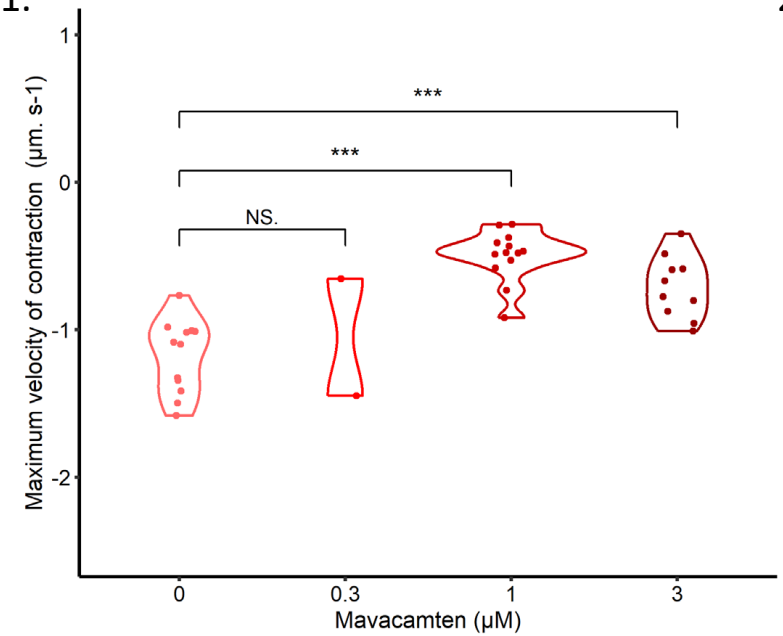

2.

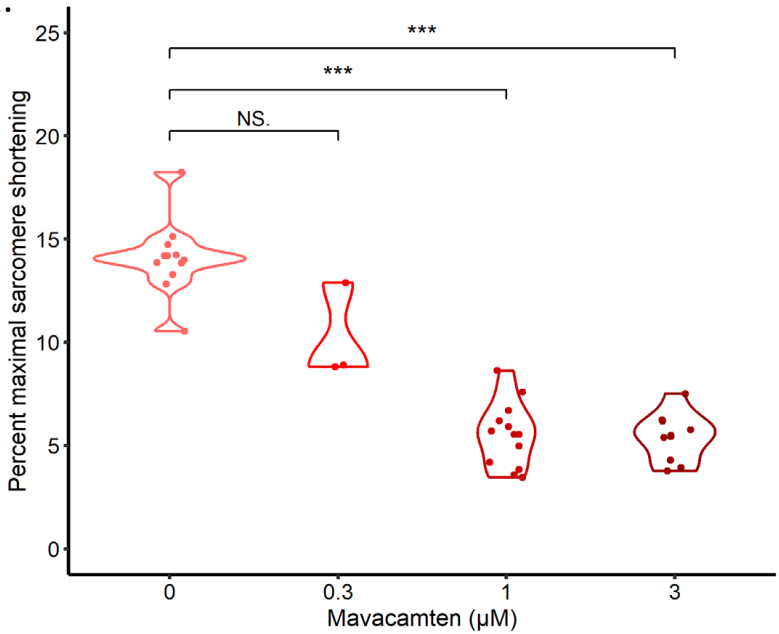

B.

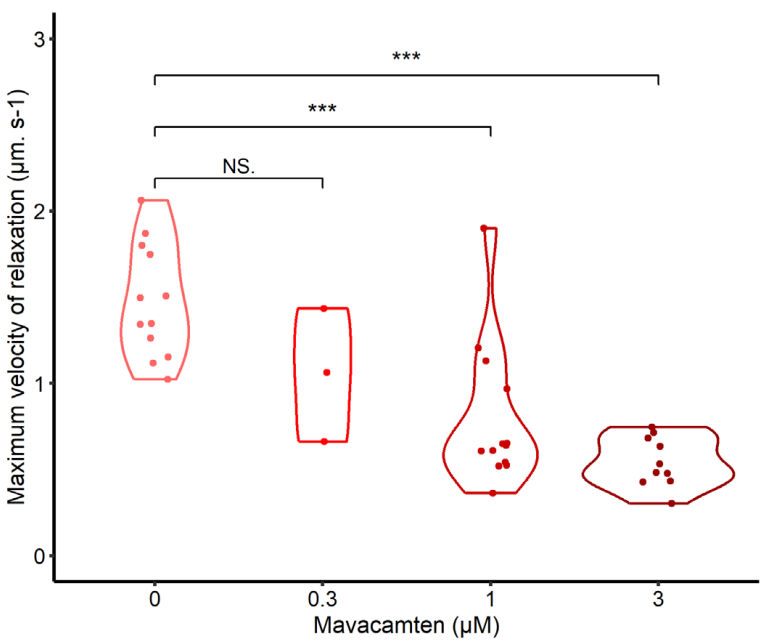

Table S1

Submissions for variant NM_001276345.2(TNNT2 c.862C-T (p.Arg288Cys)

Submitter	RCV	SCV	Clinical significance	Condition	Last evaluated	Review status	Method
Laboratory for Molecular Medicine, Mass General Brigham Personalized Medicine	RCV000036622	SCV000060277	uncertain significance	not specified	2020-11-20	criteria provided, single submitte	clinical testing
GeneDx	RCV000159322	SCV000209268	uncertain significance	not provided	2022-12-23	criteria provided, single submitte	clinical testing
Agnes Ginges Centre for Molecular Cardiology, Centenary Institute	RCV000162331	SCV000212627	uncertain significance	HCM1	2014-09-10	criteria provided, single submitte	research
Invitae	RCV000203739	SCV000261146	uncertain significance	HCM 2; DCM 1D; CM, familial restrictive, 3	2022-11-01	criteria provided, single submitte	clinical testing
Ambry Genetics	RCV000248304	SCV000318976	likely pathogenic	Cardiovascular phenotype	2023-02-23	criteria provided, single submitte	clinical testing
Center for Pediatric Genomic Medicine, Children's Mercy Hospital and Clinics	RCV000159322	SCV000511738	uncertain significance	not provided	2016-07-29	criteria provided, single submitte	clinical testing
ARUP Laboratories, Molecular Genetics and Genomics, ARUP Laboratories	RCV000159322	SCV000605411	uncertain significance	not provided	2022-09-16	criteria provided, single submitte	clinical testing
Molecular Diagnostic Laboratory for Inherited Cardiovascular Disease, Montreal Heart Institute	RCV000148898	SCV000747995	pathogenic	Primary familial HCM	2017-07-20	criteria provided, single submitte	clinical testing
Equipe Genetique des Anomalies du Developpement, UniversitÃ© de Bourgogne	RCV000755702	SCV000883136	uncertain significance	DCM 1D	2018-11-21	criteria provided, single submitte	clinical testing
Center for Human Genetics, University of Leuven	RCV000768493	SCV000886798	likely pathogenic	HCM	2018-10-31	criteria provided, single submitte	clinical testing
Color Diagnostics, LLC DBA Color Health	RCV000771167	SCV000903051	uncertain significance	Cardiomyopathy	2021-04-29	criteria provided, single submitte	clinical testing
Mendelics	RCV000013222	SCV001135514	uncertain significance	HCM2	2019-05-28	criteria provided, single submitte	clinical testing
CHEO Genetics Diagnostic Laboratory, Children's Hospital of Eastern Ontario	RCV000771167	SCV001333649	uncertain significance	Cardiomyopathy	2021-08-20	criteria provided, single submitte	clinical testing
Women's Health and Genetics/Laboratory Corporation of America, LabCorp	RCV000036622	SCV001362086	uncertain significance	not specified	2019-02-19	criteria provided, single submitte	clinical testing
Johns Hopkins Genomics, Johns Hopkins University	RCV000203739	SCV001425368	uncertain significance	HCM 2; DCM 1D; CM, familial restrictive, 3	2020-05-11	criteria provided, single submitte	clinical testing
Institute of Human Genetics, University of Leipzig Medical Center	RCV000755702	SCV001440698	uncertain significance	DCM 1D	2019-01-01	criteria provided, single submitte	clinical testing
Laboratory of Medical Genetics, National & Kapodistrian University of Athens	RCV000755702	SCV001976864	likely pathogenic	DCM 1D	2021-10-06	criteria provided, single submitte	clinical testing
OMIM	RCV000013222	SCV000033469	pathogenic	HCM 2	1999-07-22	no assertion criteria provided	literature only
Blueprint Genetics	RCV000157540	SCV000207286	uncertain significance	Costello syndrome	2013-08-28	no assertion criteria provided	clinical testing
Stanford Center for Inherited Cardiovascular Disease, Stanford University	RCV000036622	SCV000280532	uncertain significance	not specified	2013-05-23	no assertion criteria provided	clinical testing
Diagnostic Laboratory, Department of Genetics, University Medical Center Groningen	RCV000159322	SCV001743238	likely pathogenic	not provided		no assertion criteria provided	clinical testing
Clinical Genetics, Academic Medical Center	RCV000159322	SCV001920549	likely pathogenic	not provided		no assertion criteria provided	clinical testing
Joint Genome Diagnostic Labs from Nijmegen and Maastricht, Radboudumc and MUMC+	RCV000159322	SCV001959218	pathogenic	not provided		no assertion criteria provided	clinical testing
Clinical Genetics DNA and cytogenetics Diagnostics Lab, Erasmus MC, Erasmus Medical Center	RCV000159322	SCV001963708	likely pathogenic	not provided		no assertion criteria provided	clinical testing

Figure S1

```
Human       AIDHLNEDQLREKAKELWQSIYNLEAEKFDLQEKFKQQKYEINVLRNRINDNQKVSK---    286
Bovine      AIDHLNEDQLREKAKELWQMIYDLEAEKFDLQEKFKQQKYEINVLRNRINDNQKVSK---    273
Rabbit      AIDHLNEDQLREKAKELWQSIYNLEAEKFDLQEKFKQQKYEINVLRNRINDNQKVSK---    289
Rat         AIDHLNEDQLREKAKELWQSIHNLEAEKFDLQEKFKQQKYEINVLRNRINDNQKVSK---    287
Mouse       AIDHLNEDQLREKAKELWQSIHNLEAEKFDLQEKFKQQKYEINVLRNRINDNQKVSK---    289
chicken     NIDHLSEDKLRDKAKELWQTIRDLEAEKFDLQEKFKRQKYEINVLRNRVSDHQKVKGSKA    290
Zebrafish   DIDNANESALREKAKELWSWMRELEAEKFELQYQFGKQKYEINVLRNRVSDHQKTSKRTK    277
             **: .*. **:******. : :******:** :* :***********:.*:**.

            R278
Human       TRGKAKVTGRWK 298
Bovine      TRGKAKVTGRWK 285
Rabbit      TRGKAKVTGRWK 301
Rat         TRGKAKVTGRWK 299
Mouse       TRGKAKVTGRWK 301
chicken     ARGKTMVGGRWK 302
Zebrafish   -RGLRK------ 282
             **
```

Figure S2

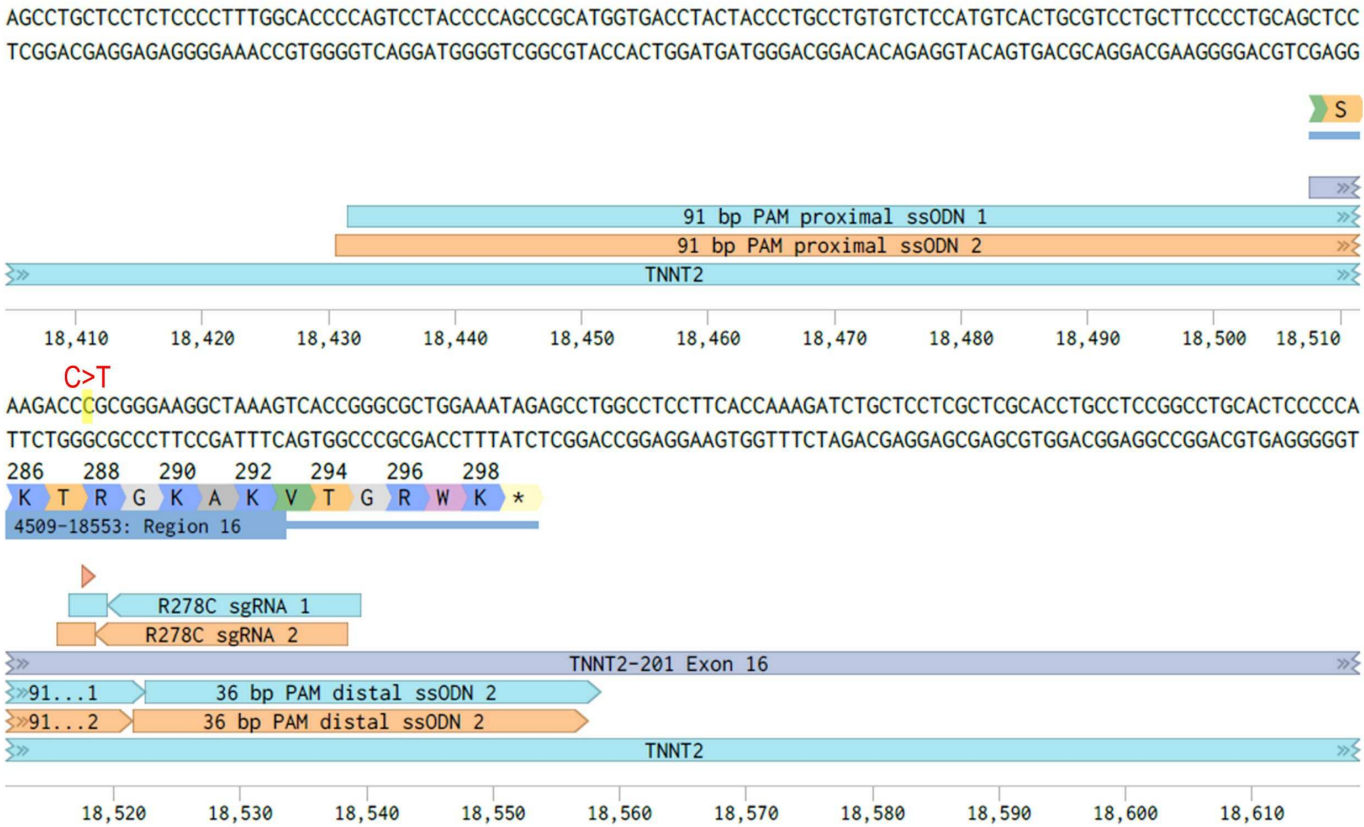

Design 1
iPS(IMR90)-4
R278C *TNNT2*

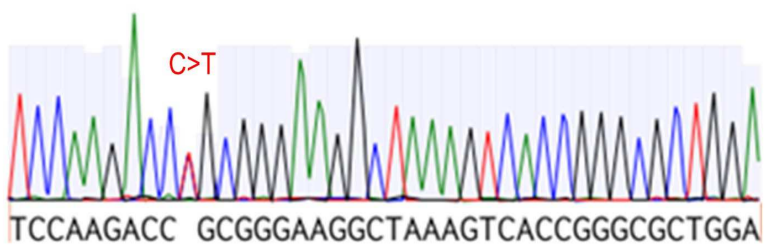
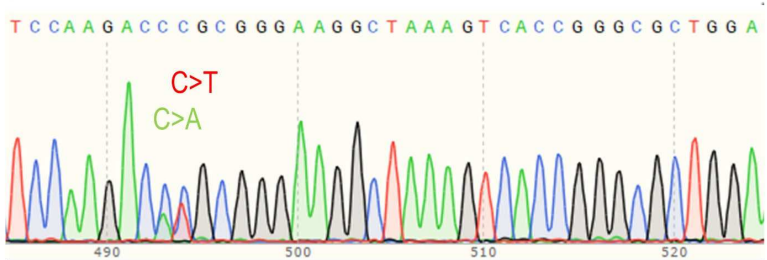
Design 2
AICS-0075 cl.87
R278C *TNNT2*